# Understanding Extreme Rainfall in the Sahel of Southwestern Mali

Edward K. Vizy\* and Kerry H. Cook\*\*

Department of Earth and Planetary Sciences

Jackson School of Geosciences, The University of Texas at Austin

Austin, TX 78712

# **Published in Climate Dynamics**

This preprint has not undergone any post-submission improvements or corrections. The Version of Record of this article is published in Climate Dynamics, and is available online at https://doi.org/10.1007/s00382-024-07241-y

The citation for this work is as follows:

Vizy EK, Cook KH (2024) Understanding extreme rainfall in the Sahel of Southwestern Mali. Climate Dynamics. https://doi.org/10.1007/s00382-024-07241-y

\* Corresponding author ORCID ID: 0000-0002-5019-2819
\*\* Co-author ORCID ID: 0000-0001-9270-4395

e-mail: ned@jsg.utexas.edu

e-mail: kc@jsg.utexas.edu

1

**Abstract** 

West African Sahel extreme rainfall events cause flooding and property damage, and some areas are more

prone to their occurrence. One favorable region is southwestern Mali. NASA IMERG precipitation and

ERA5 reanalysis data are used to examine the most extreme boreal summer rainfall events from 2000 -

2019 over southwestern Mali to understand why they form, and to explain why this region has frequent

activity. Events are sorted into 4 types based on the timing of the peak rainfall (before or after 00Z) and

the associated mid-tropospheric circulation pattern (coastal low or ridge). The coastal low types are

associated not with an increase of the low-level inflow of moisture into southwestern Mali, but a weakening

of the mid-level westward transport of moisture out of the region. The timing and longevity of the event

depends on whether there is a second low to the east in the southern storm track. The coastal ridge types

are associated with a build-up of warm, dry air over the western Sahara that leads to a stronger temperature

inversion cap over southwestern Mali, allowing instability to build beneath the cap. How fast the cap

dissipates and whether there is synoptic activity to the east in the southern or northern storm track

determines when convective activity occurs. Thus, southwestern Mali is exposed to coastal lows and ridges

in addition to the Saharan heat low and the summer southern storm track for African easterly wave

disturbances. The confluence of these factors makes southwestern Mali a region conducive for convective

rainfall activity.

Keywords: extreme rainfall, West African Sahel, atmospheric capping inversion, African easterly wave

#### 1. Introduction

Extreme rainfall events carry high impacts, with heavy rains often leading to flooding and strong winds causing property damage. These events can happen anywhere, but some regions favor their occurrence. Southwestern Mali is one such region that favors extreme 24-h rainfall totals. Vizy and Cook (2022; hereafter VC22) reported that about one-third of the top 100 rainfall events in the West African Sahel from 2000 – 2019 occur in this region.

The purpose of this study is to utilize satellite-derived rainfall estimates and atmospheric reanalysis data to better understand southwestern Mali extreme rainfall events. We identify common factors among the extreme rainfall events over this region that are most influential for storm development to aid forecasting and climate prediction, and to explain why this region is especially favorable for extreme rainfall.

Background is provided in Section 2. Section 3 describes the datasets and methodology, while the results are presented in Section 4. Conclusions are presented in section 5.

### 2. Background

Heavy rainfall events frequent the boreal summer West African Sahel as well-organized mesoscale convective systems (MCSs) and squall lines form over this semi-arid region and travel westward. These convective systems occasionally produce very high rainfall rates, causing floods that can damage property and agriculture, disrupt transportation routes, and result in the loss of lives (DiBaldassarre et al. 2010; Tschakert et al. 2010; Panthou et al. 2014; Anash et al. 2020). Impacts are compounded in urban areas where the population is denser, and the drainage infrastructure can be inadequate to nonexistent (Egbinola et al. 2017; Mahmood et al. 2017).

West African Sahel extreme rainfall events have changed over the past 40 years. There has been a significant increase in their frequency (Chagnaud et al. 2022; Saley and Salack 2023) as rainfall producing storms have become more intense and better organized (Taylor et al. 2017; Tramblay et al. 2020; Kleinet al. 2021). Flooding has increased as the storms become more frequent and destructive (Elagib et al. 2021; Fofana et al. 2022; Chahinian et al. 2023), although some of the increase in flood disasters is associated

with landuse/landcover changes associated with a quickly growing population (Sougué et al. 2023) as over the last 40 years, the population of the West African Sahel nations of Senegal, Gambia, Mauritania, Mali, Burkina Faso, and Niger has increased from around 27 million in 1979 to 92 million in 2021 (United Nations 2022). These changes in storm intensity and frequency are projected to continue (Han et al. 2019; Kendon et al. 2019; Fitzpatrick et al. 2020; Saley and Salack 2023).

Numerous factors can influence a convective storm's development. Most widely understood is that a storm needs a conditionally unstable environment with some sort of lifting mechanism to trigger the development of deep convection (Doswell et al. 1996). Over the West African Sahel during the boreal summer, the low-level inflow of moist, tropical air from the Gulf of Guinea and tropical Atlantic (Cook 1997; Thorncroft et al. 2011; Vizy and Cook 2018) is overlain by dry air at mid-levels associated with outflow from the Saharan heat low (Thorncroft and Blackburn 1999; Lavaysse et al. 2009; Engelstaedter et al. 2015), yielding a potentially unstable environment. If the dry air layer is warmer than the near surface atmosphere it can form a temperature inversion cap. The cap inhibits convective development until it is "broken" by either vertical mixing associated with daytime planetary boundary layer growth due to surface heating or by some dynamical forcing mechanism that promotes low-level convergence and rising vertical motion (Parker et al. 2005; Cuesta et al. 2009). Over West Africa examples of dynamical lifting mechanisms include cold pool outflow boundaries (Redelsperger and Lafore 1988; Marsham et al. 2013; Provod et al. 2016), interactions of the flow with topography (Tetzlaff and Peters 1988; Laing et al. 2008; Vizy and Cook 2023), frontal/airmass boundaries such as West African squall lines (Peters and Tetzlaff 1988; Rowell and Milford 1993; Fink and Reiner 2003) and the Intertropical front/Intertropical discontinuity/dryline (Eldridge 1957; Lélé and Lamb 2010; Vizy and Cook 2018, 2019), and African easterly waves (AEWs; Carlson 1969a,b; Burpee 1972; Reed et al. 1977). AEWs help to organize convective activity into larger storm complexes, mainly mesoscale convective systems (MCSs), and they influence horizontal and vertical wind shear (Rowell and Milford 1993; Mohr and Thorncorft 2006). There are two preferred storm tracks for AEWs over northern Africa, a southerly storm track between 8°N - 15°N and a northerly storm track north of 15°N (Diehiou et al. 1999; Fink and Reiner 2003; Hsieh and Cook

2005, 2008). For the former, convective development tends to occur west of AEW troughs (Burpee 1972; Tetzlaff and Peters 1988) while, for the latter, it tends to occur to the east of troughs where the southerly flow of moist air is enhanced (Duvel 1989; Fink and Reiner 2003).

Recent progress in understanding extreme rainfall events over West Africa includes the work of Knippertz and Martin (2005), who examined three cold season extreme events and found that extratropical/tropical dynamical interactions generate a moisture plume from the Atlantic into the continent that was integral into the occurrence of heavy rainfall. Numerous studies (Galvin 2010; Cornforth et al. 2017; Engel et al. 2017; Lafore et al. 2017a; Miller et al. 2022) have examined the 1 September 2009 event over Ouagadougou, Burkina Faso, one of the most extreme rainfall events recorded over the Sahel. This event was associated with an initial strong, slow moving AEW disturbance trailed by a second AEW in the southern storm track. These disturbances combined to produce strong loading of moisture over Burkina Faso and dynamical forcing that aided in the development of two MCSs that hit Ouagadougou within 6 hours that yielded 263 mm of rain. The slow propagation of the AEW was associated with AEW breaking (Galvin 2010; Cornforth et al. 2017) which helped contribute to the high rainfall totals. Fall et al. (2020) investigated the 26 August 2017 extreme rainfall event over Linguère, Senegal, that produced 218.6 mm of rain. This morning event was associated with the development of an MCS in the prior afternoon ahead of an approaching AEW disturbance that slowed down as it approached the West African coast. Chahinian et al. (2023) examined the 16 May 2019 heavy rainfall event over Bamako, Mali. A short-lived MCS formed in the early morning hours in association with a mid-level AEW disturbance in the northern storm track.

VC22 evaluated the top 10 wettest 24-h events between 2000 – 2019 over the West African Sahel. They note similarities among some of the events, including the role of AEWs that transport moisture into the region and the potential importance of anticyclonic ridging along the coast that slows the approaching AEWs. In an examination of two rainfall events over northern Nigeria/Niger, Vizy and Cook (2023) find that both events develop in anomalously moist environments, but that the environments do not necessarily have to be highly unstable for extreme rainfall to occur. Other factors such as cold pool outflow boundaries and circulation interaction with local terrain features support storm development.

These case studies highlight the complexities associated with understanding the development of extreme rainfall events. The challenge is to understand which mechanisms are important for extreme rainfall events. To our knowledge VC22 is a first attempt to take a more holistic view of extreme rainfall events over the West African Sahel to generalize common characteristics. However, these results suggest that a more regionalized approach that considers a larger number of events would be beneficial.

### 3. Datasets & Methodology

### 3.1 Datasets

Two datasets are utilized for this study. For rainfall we use the NASA Long-term Integrated Multi-satellite Retrievals for Global Precipitation measurement Version 06B final run (IMERG; Huffman et al. 2020). This product has 0.10° spatial resolution providing rainfall estimates every 30-minutes from 2000 – present. IMERG is used to select and classify extreme events.

The European Centre for Medium-Range Weather Forecasts Reanalysis v5 (ERA5; Hersbach et al. 2020) is examined to relate the selected events to changes in the atmosphere. ERA5 is a 5<sup>th</sup> generation atmospheric reanalysis that provides gridded 0.25° resolution hourly output of atmospheric and surface fields back to 1940. Past studies (Danso et al. 2019; Vizy and Cook 2019, 2022, 2023; Li et al. 2020) have shown that ERA5 can reasonably represent storm development processes, including over Africa.

# 3.2 Methodology

A detailed explanation of how IMERG is used to identify extreme rainfall events over the West African Sahel region (8.05°W – 12.95°E and 12.05°N – 17.95°N) between 2000 – 2019 is presented in VC22. Here we summarize the approach. 12Z – 12Z 24-hr rainfall totals are calculated for every gridpoint in the region to find the top 100 wettest "independent" events over the 20 years. To be "independent" a gridpoint under consideration cannot be associated with a rainfall event that has already been identified as having a higher 24-h rainfall total on the same day within 500 km of the gridpoint. This criterion is used to account for heavy rainfall events impacting a spatial area greater than a single gridpoint without double

counting the event. Events are referenced by the date and location (latitude, longitude) where the maximum 24-h rainfall occurred. Table 1 in VC22 lists the events, and Fig. 1 shows their locations.

Here we study a subset of the extreme events identified in VC22, namely, the cluster of extreme storms that occurred over southwestern Mali –located at 8.05°W – 5.05°W and 12.05°N – 14.95°N (blue box in Fig. 1). This area coincides with the heart of the Niger River delta over southwestern Mali. These 31 storms occurred in the southwest corner of the VC22 analysis region, comprising one-third of the extreme events identified over their larger analysis region. The cluster region includes Bamako, the largest urban area in Mali with a population greater than 2.9 million. Fig. 1 shows their locations while Table 1 provides more detail on each event.

To examine similarities among the 31 storms and the environments in which they form, compositing is used. We first eliminate the 7 storms that occur outside of the boreal summer monsoon season, defined here as June 15 through September 15 (Thorncroft et al. 2011; Zhang et al. 2014; Cook 2015). This reduces the effects of seasonality on the large-scale environment.

Storms are then sorted according to the time of day of the peak rainfall rate. Events that produce maximum rainfall prior to 00Z are termed PM events, and those with rainfall maxima after 00Z are termed AM events. About half of the events fall into each category (Table 1). Events are sorted in this manner to better distinguish the processes associated with the storms as PM events have a stronger direct relationship with daytime heating while AM events in the early morning hours will not. Given that the population of extreme events we are considering for this region is small (23 events), this limits the extent to which we can narrow down this temporal window more than into 12-h periods.

The final criterion uses the mid-tropospheric synoptic pattern characteristics to further sort the extreme rainfall events. An examination of each of the 24 storms indicates that all but two are associated with either a mid-tropospheric anomalous coastal ridge or an anomalous coastal low between 15°N - 20°N prior to the maximum rainfall rate. This is the final sorting before compositing, leaving four storm classifications, namely, PM anomalous coastal low (Type A; 5 events), PM anomalous coastal ridge (Type B; 6 events), AM anomalous coastal ridge (Type C; 4 events), and AM anomalous coastal low (Type D; 7

events). The two events (5-6 August 2019 and 24-25 August 2011) that do not fit into any of these categories are dropped from the analysis because the goal is to understand commonalities among storms in this region. (The 5-6 August 2019 event is associated with a mid-tropospheric anomalous trough/ridge pattern well off the coast at around  $25^{\circ}\text{W}$ , while the 24-25 August 2011 event is associated with a dual anomalous low pattern again well off the coast centered near  $30^{\circ}\text{W}$ .)

For compositing, events are aligned such that  $t_0$  is 12Z on the date of the event provided in Table 1. For example, for event #1 in Table 1  $t_0$  is 12Z 05 July 2001. This is appropriate for our method because events have already been sorted based on when the maximum rainfall rate occurs so the timing of the extreme rainfall events will be aligned usually within a few hours of one another for the PM and AM events. With this alignment, hourly composites are formed beginning 12 hours prior to  $t_0$  and extending up to 24 hours after  $t_0$ .

Figure 2 shows the 4 composite types analyzed below as indicated by the ERA5 700 hPa streamline anomalies at composite time  $t_0$  (12Z). Anomalies are calculated as the difference between the composite mean for a given type and its weighted climatology. A weighted climatology is used to reduce effects of seasonality (Vizy and Cook 2009). In this approach for each of the given events that make up the composite field, the month is noted and used to weight the climatological mean. For example, the Type A composite is comprised of 2 July, 2 August, and 1 September events (Table 1). Thus, the weighted climatology (*WC*) for Type A is:

$$WC = \frac{2}{5}Clim_{Jul} + \frac{2}{5}Clim_{Aug} + \frac{1}{5}Clim_{Sep}$$
 (1)

where  $Clim_{Jul}$ ,  $Clim_{Aug}$ , and  $Clim_{Sep}$  are the 2000 – 2019 monthly climatological values (2000 – 2019) at the selected time of day for July, August, and September, respectively.

The type A (PM Coastal low) mid-tropospheric pattern (Fig. 2a) includes anomalous low at 16°W and 19°N and anomalous ridging located offshore near 15°W and 4°N at 700 hPa. For Type B (PM Coastal ridge; Fig. 2b) an anomalous anticyclone is at 16°N and 13°W and is trailed by anomalous low at 10°N and 0°E. Type C (AM Coastal ridge; Fig. 2c) also includes anomalous coastal ridging with an anticyclone at

28°N and 12°W whose axis extends equatorward to 15°N. To the east of this feature is an anomalous low at 22°N and 1°W. Finally, Type D (AM Coastal low; Fig. 2d) consists of a pair of anomalous cyclones, one centered at 16°N and 19°W and the other located at 13°N and 1°E.

Note the decisions made above for defining the different composite types are subjective in nature and other methods could be utilized instead. This needs to be kept in mind when interpreting the results that follow in the next section.

#### 4. Results

# 4.1 Type A: PM Coastal Low Event

Figure 3a shows the 06Z ( $t_0 - 6$  h) 750 hPa geopotential height and wind anomalies on the morning prior to the event. An anomalous low is centered over western Mauritania with heights significantly lower by 10 - 15 m. This anomalous low indicates a mid-latitude trough that extends southward into the subtropics over the eastern North Atlantic and Iberian Peninsula east of the North Atlantic anticyclone. The positive height anomalies to the south near the Sierra Leone/Liberian coast are smaller in magnitude (< 5 m) and are not significant, however the anomalous flow between these two circulation features is significant, particularly over southwestern Mali and Burkina Faso. Climatologically, mid-tropospheric flow is easterly over southwestern Mali during the boreal summer at this time of day associated with the African easterly jet (AEJ; Burpee 1972; Cook 1999; Thorncroft and Blackburn 1999), so this anomalous pattern indicates a weakening of the mid-level zonal easterly flow west of  $0^{\circ}$ E and enhanced northerly flow over the Guinean Coast south of  $10^{\circ}$ N.

Figure 3b shows the precipitation time series at the maximum 24-h rainfall site beginning at  $t_{\theta}$  for the individual events (black lines) and the Type A composite mean (red line). The composite mean indicates that peak rainfall occurs at 13Z ( $t_{\theta}$  + 1 h) and 19Z ( $t_{\theta}$  + 7 h). In all cases the rainfall activity finishes shortly after 00Z ( $t_{\theta}$  + 12 h). The two events with earlier peaks, the 22 – 23 August 2011 and the 26 – 27 August 2005 event, are associated with a mid-level anomalous coastal low that is cut-off rather than elongated over Mauritania and northern Mali.

Fig. 3c shows the Type A composite mean precipitable water and the 600 - 925 hPa wind shear magnitude time series area-averaged over the study area (the white box in Fig. 3a) beginning at 06Z ( $t_0 - 6$  h). Compared to the weighted climatological mean there is a modest increase in precipitable water by about 1.5 mm or 3.5%, but it is not significant. The vertical wind shear is slightly weaker than the climatology throughout, but it is only significant between 14Z - 18Z and 22Z - 00Z which corresponds to after the two primary peaks in rainfall activity (Fig. 3b).

While Fig. 3c does not indicate a significant change in the moisture content of the entire atmospheric column, it is still important to look for changes at specific levels. Fig. 3d shows the Type A composite time series of the specific humidity anomaly area-averaged over the study region. Two features stand out. One is the anomalously high moisture content between 850 - 600 hPa. In this layer, specific humidity is 0.5 - 1.0 g kg<sup>-1</sup> higher than the climatology with the largest increases in late morning and late afternoon. Below 850 hPa the atmosphere is drier by 0.1 - 0.3 g kg<sup>-1</sup> at 06Z ( $t_0 - 6$  h). This low-level drying weakens by 14Z ( $t_0 + 2$  h) as the mid-level ridge breaks down over southwestern West Africa (not shown).

Fig. 3e shows the Type A composite time series of area-averaged absolute wind convergence over southwestern Mali while stippling indicates when the composite difference from the climatological mean is significant. There are two peaks in low-level wind convergence around 900 hPa, one at 08Z ( $t_{\theta}$  - 4 h) and the other around 16Z ( $t_{\theta}$  + 4 h), the latter is significant up to 850 hPa. Low-level wind convergence is briefly weaker between these peaks and is overlain by a period of mid-level (825 – 550 hPa) divergence associated with anomalous diffluent flow over southern Mali and Burkina Faso (Fig. 3a). Around 15Z ( $t_{\theta}$  + 3 h) the mid-level divergence weakens and is replaced by wind convergence by 17Z ( $t_{\theta}$  + 5 h).

In terms of atmospheric instability over southwestern Mali, composite CIN values are largest, ranging from 130 J kg<sup>-1</sup> at 12°N to near 300 J kg<sup>-1</sup> near 15°N, at 07Z ( $t_0$  – 5 h) but decrease to less than 100 J kg<sup>-1</sup> by 15Z ( $t_0$  + 3 h), coinciding with when CAPE values peak at around 1500 – 2000 J kg<sup>-1</sup> (not shown). While this amount of CAPE is favorable for thunderstorm development, it indicates that the atmosphere over the region is only marginally to moderately unstable as there is not a large build-up of CAPE due to the relatively high CIN values in the morning. Thus, Type A events are not necessarily associated with

either a strongly unstable environment (i.e., high CAPE values) or a large build-up of moisture in the entire atmospheric column (i.e., high precipitable water values) prior to development (Fig. 3c). This means that both CAPE and precipitable water are not good indicators for extreme rainfall activity for this event type consistent with Lafore et al. (2017b).

To better understand the anomalous moisture patterns, Figs. 4a – b show the composite mean 800 and 925 hPa specific humidity and wind anomalies, respectively at 10Z (t<sub>0</sub> - 2 h) when the mid-level moisture anomaly is largest (Fig. 3d). At 800 hPa (Fig. 4a) there is a widespread increase in specific humidity over much of West Africa with the largest anomalies coinciding with the location of mid-level coastal low over Mauritania. Over southwestern Mali there is a concentrated area of enhanced specific humidity coinciding with where there is a significant reduction in the easterly/northeasterly flow as indicated by the anomalous westerly wind vectors. At 925 hPa (Fig. 4b) specific humidity is lower than normal south of 15°N while there is a large increase north of 15°N over Mauritania.

By 15Z ( $t_0 + 3$  h) anomalous 800 hPa westerly flow between 10°N - 15°N remains in place (Fig. 4c) albeit it is now weaker over the study region compared to 10Z as the mid-level coastal trough has shifted westward and weakened. These circulation changes are associated with a reversal of the mid-level wind divergence at 10Z to convergence after 15Z (Fig. 3e) as the flow is now decelerating over southwestern Mali (i.e., the mid-level easterly flow is climatological east of the study region, but weaker to the west of the region). Positive specific humidity anomalies greater than 1 g kg<sup>-1</sup> are more expansive over and east of the southwestern Mali.

At 925 hPa (Fig. 4d) the lower atmosphere remains drier than normal at 15Z over southwestern Mali with no evidence of the low-level horizontal flow transporting more moisture into the area. To the west anomalous southwesterly flow associated with the West African westerly jet (WAWJ; Grodsky et al. 2003; Pu and Cook 2010; Liu et al. 2020) transports low-level moisture into West Africa, however this moisture is directed northward into the western Sahara.

Overall, Fig. 4 indicates that the circulation associated with the coastal low weakens the mid-tropospheric easterly flow over West Africa between 10°N - 15°N thereby reducing the mid-level moisture

transport out of southwestern Mali. While this aids in the build-up of moisture over the area, we must still consider the vertical transport of moisture. Fig. 5a shows the time series of area-averaged vertical p-velocity and zonal wind over the region from the weighted climatology, while Fig. 5b shows the same fields for the Type A composite.

The Type A composite (Fig. 5b) has numerous differences from climatology (Fig. 5a). This includes a deeper westerly flow layer and the AEJ morning maximum is about 2 m s<sup>-1</sup> weaker than climatology. This change in the zonal flow coincides with stronger upward vertical motion over the region before (06Z – 10Z) and after (14Z – 17Z) the morning AEJ maximum supported by strong low-level wind convergence (Fig. 3e). This indicates that the enhanced low-level wind convergence is associated with increased rising vertical motions that transport moist, low-level air upward over the region during the morning prior to the event. At mid-levels this moist air remains over the region due to the reduced outflow via AEJ as the jet is weaker. Rising vertical motions are only found significant between 16Z – 18Z near 500 hPa shortly before the time of peak rainfall activity (Fig. 3b) and coinciding with when there is significant low-level wind convergence (Fig. 3e). While this is not too surprising given the noisy nature of the vertical velocity field and the small composite sample size, caution should be taken when interpreting these results relative to other composite fields where the significance is more robust.

Thus, Type A is not directly associated with a remote horizontal moisture transport mechanism (e.g., a low-level jet and/or moisture plume from the North Atlantic) that loads the atmospheric column with moisture over southwestern Mali. Rather its moisture source is regional/localized, namely enhanced low-level vertical mixing of moist air upward combined with reduced mid-level moisture transport out of the region associated with a weaker AEJ. Extreme rainfall is dynamically forced in the afternoon (Fig. 3b) as the mid-level anomalous low shifts westward (Figs. 4a and 4c) and mid-level wind convergence increases over the area (Fig. 3e).

### 4.2 Type B: PM Coastal Ridge Event

Figure 6 is like Fig. 3, except it shows composites for PM coastal ridge events. Fig. 6a shows the Type B composite 750 hPa geopotential height and wind anomalies at 06Z ( $t_0$  - 6 h) prior to the event. Positive height anomalies along the coast are significant as is the anomalous northerly flow over West Africa near  $10^{\circ}$ W. This anomalous pattern signifies a stronger than normal North Atlantic anticyclone over the eastern North Atlantic and northwestern Sahara. Additionally, there is an anomalous low east of the Mali analysis region, but the height anomalies are not significant as this feature is still early in its development at this time (not shown).

Fig. 6b shows the precipitation profiles. At first glance the composite mean peak occurs around 19Z ( $t_0 + 7$  h) but there appears to be multiple peaks between 15Z ( $t_0 + 3$  h) and 03Z ( $t_0 + 15$  h). While it is hard to discern from Fig. 6b, closer inspection of the individual events indicates that 4 of the 6 events have most of their convective activity occurring between 18Z ( $t_0 + 6$  h) to 22Z ( $t_0 + 10$  h). It is two events, the 07 – 08 August 2012 and the 26 – 27 August 2005 events that complicate matters. Both of these events have an early afternoon peak between 14Z – 16Z which is the maximum for the 24-h period (Table 1), followed by a second peak around 01Z - 02Z, and in the case of the 07 – 08 August event a third peak around 08Z. Furthermore, the anomalous low east of Mali is stronger compared to the other 4 Type B cases (not shown), suggesting that the development of additional convective activity is likely associated with the development of this circulation feature.

In terms of atmospheric moisture content, there is not a significant increase in precipitable water over the study area during the afternoon for the Type B composite (Fig. 6c). Precipitable water does, however, gradually increase after 06Z ( $t_0 - 6$  h) by 1.5 - 2.5 mm or 2.5 - 5% compared to climatology, and these increases are greater than those for the Type A events (Fig. 3c). Vertical wind shear is 4 - 6 m s<sup>-1</sup> stronger than climatology the entire day, but it is only significant around 09Z h, coinciding with when the diurnal peak intensity of the AEJ occurs (Fig. 5a), and between 18Z ( $t_0 + 6h$ ) – 20Z ( $t_0 + 8h$ ) when rainfall is at peak intensity in the composite mean (Fig. 6b).

Fig. 6d shows the Type B time series of the area-averaged specific humidity anomaly over the study region. Unlike Type A, Type B is associated with a significant increase in both low- and mid-level moisture between 06Z ( $t_0 - 6$  h) and 21Z ( $t_0 + 9$  h) as well as a significant reduction in moisture at 600 hPa between 09Z ( $t_0 - 3$  h) and 12Z ( $t_0$ ), the latter coincides with the AEJ maximum during the diurnal cycle (Fig. 5a) which is approximately 2 m s<sup>-1</sup> stronger than climatology (not shown).

Fig. 6e shows the Type B composite time series of area-averaged absolute wind convergence over southwestern Mali. The cross section indicates a pattern of low-level wind convergence from the surface to 800 hPa and mid-level divergence from 800 hPa and 650 hPa between 06Z ( $t_0$  – 6 h) and 14Z ( $t_0$  + 2 h). There also is strong convergence above 900 hPa between 15Z ( $t_0$  + 3 h) – 21Z ( $t_0$  + 9 h) associated with when the strongest convective activity occurs (Fig. 6b).

To understand the differences between the low- and mid-levels, Figs. 7a - b show the 10Z ( $t_0 - 2$  h) geopotential height and wind anomaly composites for Type B at 750 hPa and 850 hPa, respectively. At 10Z the anomalous coastal ridge is identifiable at both 750 hPa (Fig. 7a) and 850 hPa (Fig. 7b) with anomalous northerly flow along its eastern flank at  $10^{\circ}$ W, and anomalous easterly flow along its southern flank between  $7^{\circ}$ N -  $12^{\circ}$ N. The anomalous low in the southern storm track at 750 hPa is located at  $10^{\circ}$ N and  $3^{\circ}$ E, but at 850 hPa this feature is barely identifiable. Instead, over northern Mali and eastern Mauritania there is a more spatially robust anomalous low at 850 hPa that is not apparent at 750 hPa. This feature is associated with anomalous westerly/northwesterly flow between  $10^{\circ}$ N -  $15^{\circ}$ N over southern Mali that is directed towards the location of the mid-level southern storm track low which is a slow-moving developing AEW that is propagating westward at 5.77 m s<sup>-1</sup>.

This anomalous circulation feature over northern Mali at 850 hPa signifies an intensification of the Saharan thermal low (Knippertz and Fink 2008; Lavaysse et al. 2009). Fig. 7c shows the Type B composite 850 hPa temperature anomalies at 10Z, while Fig. 7d shows the 925 hPa specific humidity anomalies. The strong northerly low-level flow associated with the eastern flank of the coastal ridge is associated with a significant warming (Fig. 7c) and drying (Fig. 7d) of the low-level western Saharan environment with 850 hPa temperatures more than 2 K warmer and 925 hPa specific humidity 2 g kg<sup>-1</sup> lower than climatology.

Over southwestern Mali there is some warming, but the strongest warming remains north of 15°N. There is also a significant increase in low-level specific humidity between 10°N - 15°N over much of southern and southeastern Mali and northern Burkina Faso associated with enhanced low-level inflow into the thermal low during the night prior (not shown), consistent with Parker et al. (2005).

Figs. 7e and 7f show the 10Z Type B composite CAPE and CIN values, respectively. Upstream of the analysis region CAPE values are up to 2700 J kg<sup>-1</sup> over central Mali along the Mali/Burkina Faso border while CIN values are greater than 200 J kg<sup>-1</sup> suggesting a strong atmospheric cap is in place. This favors the build-up of CAPE due to an increase in low-level moisture (Fig. 7d) combined with the mid-level advection of warmer (and drier) air (Fig. 7c) from the western Sahara. Over the analysis region (red box) CAPE values range between 1000 – 2000 J kg<sup>-1</sup> while there is an area of relatively lower CIN values (100 – 200 J kg<sup>-1</sup>) indicating a weak spot in the capping inversion.

Fig. 7g shows the Type B 10Z ( $t_0-2$  h) composite vertical cross-section of temperature anomalies averaged between  $5^{\circ}W$  -  $8^{\circ}W$ . North of  $18^{\circ}N$  warming is strongest with temperature anomalies greater than +0.8 K extending up to 750 hPa. Some of this warm air is advected by the anomalous northerly flow equatorward over the southern Sahel as mid-level temperatures between  $10^{\circ}N$  -  $15^{\circ}N$  warm by 0.4-0.6 K. There is also evidence of a temperature inversion cap around 900 hPa, but it is confined between  $16^{\circ}N$  -  $18^{\circ}N$  which is north of the study region.

By 15Z ( $t_0 + 3$  h) the 750 hPa (Fig. 8a) anomalous ridge is oriented right along the coast while the anomalous low is centered over Burkina Faso. There is still anomalous northerly flow north of  $10^{\circ}$ N over western Mali, while south of  $10^{\circ}$ N anomalous flow is easterly. At 850 hPa (Fig. 8b) the ridge axis shifted westward to  $18^{\circ}$ W. The anomalous low over northern Mali remains in place while the southern storm track low has become more spatially robust and is now centered over Burkina Faso with significant anomalous flow directed towards its center. The 15Z temperature (Fig. 8c) and specific humidity (Fig. 8d) anomalies largely resemble those from 10Z but with the strongest warming and drying over northern Mali/western Mauritania now shifted a few degrees equatorward to  $18^{\circ}$ N and the warming between  $10^{\circ}$ N -  $15^{\circ}$ N having weakened. The atmosphere remains extremely unstable over Mali with CAPE values over 3000 J kg<sup>-1</sup> (Fig.

8e) to the north and east of the study region in an area where the low-level moisture loading is greatest while CIN values have decreased everywhere from their 10Z values by the afternoon (Fig. 8f) indicating that the capping inversion over the analysis region has dissipated by the early afternoon (Fig. 8g).

Unlike Type A, the Type B extreme rainfall event is associated with the development of a highly unstable environment over southern Mali as coastal ridging promotes warmer and drier conditions that intensify the Saharan thermal low over the western Sahara. This in turn enhances the low-level westerly/southwesterly flow of moisture into southern Mali along the thermal low's southern flank the night prior to the event. Strong afternoon convection develops over the area as there is an ample moisture source and enough low-level wind convergence associated with the developing AEW in the southern storm track behind the ridge to trigger the convective activity in the absence of an atmospheric capping inversion.

# 4.3 Type C: AM Coastal Ridge Event

Fig. 9a shows the Type C composite 750 hPa geopotential height and wind anomalies at 18Z ( $t_0 + 6$  h). The anomalous ridge is positioned along  $15^{\circ}$ W with anomalous northerly flow and easterly flow along its northern and southern flanks, respectively. This anomalous ridging signifies an eastward extension of the North Atlantic anticyclone over the northwestern Sahara. Over northern Mali, southern Algeria, and western Niger heights are lower helping to strengthen the zonal height gradient over the western Sahel. This low is a developing feature over this region rather than a westward propagating AEW over the northern Sahel.

Fig. 9b shows the precipitation time series for the individual composite members and the composite mean at the maximum 24-h rainfall sites. All 4 events have a distinct peak in the rainfall between 01Z ( $t_{\theta}$  + 13 h) and 03Z ( $t_{\theta}$  + 15 h) with much of the rainfall activity over with by 06Z ( $t_{\theta}$  + 18 h). Two cases, the 14–15 July 2007 and the 19–20 July 2010 events, have rainfall commencing in the evening prior, however the associated rainfall rates are about one-third the magnitude of the composite mean peak at 02Z.

Fig. 9c shows the Type C composite mean precipitable water and vertical wind shear area-averaged over the study region. Prior to  $18Z (t_0 + 6 h)$  the atmospheric column is drier than the climatological mean,

but this quickly changes after 20Z ( $t_0 + 8$  h) as the atmospheric moisture content increases to 51 mm by 01Z ( $t_0 + 13$  h) which is 3 mm greater than climatology. This nighttime increase in moisture is significant. The vertical wind shear is significantly higher during the afternoon and night. It starts at around 6 m s<sup>-1</sup> higher at 12Z ( $t_0$ ) and gradually decreases to 2 m s<sup>-1</sup> higher by 06Z ( $t_0 + 18$  h).

Fig. 9d shows the time series of the specific humidity anomaly over southwestern Mali. At 18Z ( $t_{\theta}$  + 6 h), there is a significant increase in the specific humidity below 700 hPa and a decrease above 700 hPa associated with the anomalous northerly flow around the anticyclone's eastern flank. This mid-level drying persists to 23Z ( $t_{\theta}$  + 11 h) when conditions become wetter, coinciding with when precipitable water significantly increases (Fig. 9d).

Fig. 9e shows the time series of area-averaged absolute wind convergence over the study region. While wind convergence occurs in 900 – 600 hPa layer throughout the evening and overnight, it peaks in magnitude at 00Z ( $t_0 + 12$  h) and remains greater than  $8 \times 10^{-6}$  s<sup>-1</sup> until 06Z. This coincides with when the strongest convective activity occurs (Fig. 9b). Below 900 hPa there is low-level divergence near the surface throughout the night.

Figs. 10a - b show the Type C 750 hPa and 850 hPa geopotential height and wind anomalies at 12Z (t<sub>θ</sub>). Like Type B, the coastal ridge is associated with anomalous northerly flow along its eastern flank over Mauritania and Mali for Type C. However, unlike Type B, the western Saharan thermal low is deeper and extends into the mid-levels for Type C. This may be associated with seasonal differences between when the individual Type B and Type C events occur, as all 4 Type C events occur before 20 July, while all 6 Type B events occur after 24 July and 5 of the 6 events occur after 01 August.

Fig. 10c - d show the 12Z ( $t_0$ ) 850 hPa composite temperature and 925 hPa specific humidity anomalies, respectively. There is strong warming (> 2 K) and drying (1.5 – 2.5 g kg<sup>-1</sup>) over much of Mauritania and Mali north of 15°N. Over southwestern Mali there is an increase in 925 hPa specific humidity, but it is relatively small in magnitude (< 0.5 g kg<sup>-1</sup>) while 850 hPa temperatures are up to 1 K warmer. Additionally, CAPE values over much of southern Mali are elevated compared to the climatological normal, ranging from 1500 – 2000 J kg<sup>-1</sup> (Fig. 10e) but CIN values are greater than 200 J kg<sup>-1</sup>

<sup>1</sup> (Fig. 10f). These values indicate that the environment is only marginally to moderately unstable at 12Z  $(t_0)$  and a strong atmospheric cap is in place.

Fig. 10g shows the Type C composite cross-section of temperature anomalies area averaged between  $5^{\circ}\text{W}$  -  $8^{\circ}\text{W}$  at 12Z ( $t_0$ ). Like Type B (Fig. 6f), there is significant warming over the northern Sahel that extends up to 600 hPa and evidence that this warming is advected equatorward by the anomalous midlevel northerly flow. However, the mid-level warming over the southern Sahel is more robust as temperatures are 0.4 - 1.2 K warmer than climatology between 850 hPa and 600 hPa over  $12^{\circ}\text{N}$  -  $14^{\circ}\text{N}$  for Type C. This mid-level warming mechanism is associated with the development of a strong temperature inversion cap at 850 hPa that inhibits the afternoon convective development over southwestern Mali.

By 00Z ( $t_0 + 12 h$ ) the ridge axis has moved west and cleared the West African coast at 750 hPa (Fig. 11a) and 850 hPa (Fig. 11b) signifying a weakening of the North Atlantic anticyclone extension over the northwestern Sahara. The Saharan thermal low has also shifted west to 6°W due north of the Mali study region. Low-level anomalous flow becomes more westerly over southern Mali as this region now lies on the southern flank of the thermal low. Likewise, the strongest 850 hPa warming shifts westward over central Mauritania (Fig. 11c) while warming over the southern Sahel weakens east of 10°W. Between 10°N - 15°N there is an increase in 850 hPa specific humidity from 3°W - 13°W (Fig. 11d) associated with the enhanced low-level westerly flow on the southern flank of the thermal low that constitutes strong low-level nocturnal inflow into the thermal low below 850 hPa (Parker et al. 2005) and an intensification of the WAWJ (Pu and Cook 2010; Liu et al. 2020) into the continental interior during the nighttime hours. The added low-level moisture is associated with a marginally to moderately unstable nighttime environment over southwestern Mali as CAPE values are around 1500 - 2000 J kg<sup>-1</sup> (Fig. 11e) while CIN values over the analysis region are 100 J kg<sup>-1</sup> or less (Fig. 11f). The strong afternoon temperature inversion cap at 850 hPa over the study region has dissipated by 22Z ( $t_0 + 12 h$ ) in the composite (Fig. 11g) allowing for convective activity to now begin developing over the area.

While Type B and C events are both associated with anomalous mid-tropospheric coastal ridging, a fundamental distinction between them is that the capping inversion is stronger and does not dissipate over

southwestern Mali until the late evening hours for Type C. This inhibits convective development until the early morning hours for Type C rather than in the late afternoon like for Type B. The strong cap is associated with a stronger, deeper Saharan thermal low over the western Sahara that plays a role in supporting the advection of warmer and drier air to maintain the cap during the daytime, as well as to enhance the low-level westerly inflow of moisture into the region via the WAWJ at night along its southern flank. This delayed release of the daytime atmospheric instability combined with the significant build-up of low-level moisture yields extreme rainfall over the region after the cap dissipates. Additionally, the location of the low to the east of the region differs. For Type B the low is an approaching AEW in the southern storm track southeast of the analysis region (Fig. 2b) while for Type C the low is a developing circulation feature in the wake of the ridge over the western Sahara. The latter reinforces the southward transport of warm, dry air from the northwestern Sahara over the region helping to maintain the cap into the evening, while the former is more limited in doing so as it is located further south. This means that the dynamics of the approaching AEW for Type B helps to break down the cap much earlier in the day allowing for convective development by the afternoon.

Finally, inspection of the individual events that comprise the Type C composite (not shown) indicates that the two cases (the 14-15 July 2007 and the 19-20 July 2010 events) where convective activity commenced in the early evening are associated with stronger warming (4-6 K compared to 1-2 K for the other cases) over the Western Sahara and the capping inversion disappears by 18Z ( $t_0+6$  h). This indicates that, among other factors, how strong the capping inversion is and how quickly it dissipates are important factors to consider for the timing of the convective development for extreme rainfall events.

### 4.4 Type D: AM Coastal Low Event

Fig. 12a shows the Type D composite 700 hPa anomalous geopotential heights and winds at 18Z ( $t_0$ +6 h). An anomalous coastal low just off the Senegal coast is associated with anomalous westerly/southwesterly flow into West Africa along its southern flank. This mid-level anomalous flow splits over southwestern Mali with part of it directed northward along the eastern flank of the coastal

cyclone, while the rest is directed eastward into a mid-level anomalous low over Burkina Faso. Both lows are AEWs propagating westward at speeds of 7.58 m s<sup>-1</sup> and 8.84 m s<sup>-1</sup> for the coastal low and trailing low, respectively.

The Type D precipitation profiles at the maximum 24-h rainfall sites (Fig. 12b) indicate that there is not a preferred peak time for the 7 events. Inspection of the individual events indicates that 3 events (14 – 15 August 2003, 14 – 15 August 2010, and 23 – 24 August 2003) are associated with a single round of rainfall over the maximum site where peak rainfall occurs between 01Z ( $t_0$ +13 h) – 03Z ( $t_0$ +15 h). Peak rainfall rates for the remaining 4 events occur after 05Z ( $t_0$  + 17 h) and 3 of these events are associated with multiple rounds of rainfall activity. This difference among the events is reflected in the composite mean as there are maxima at 02Z and 09Z.

Fig. 12c shows the Type D composite mean vertical wind shear and precipitable water over southwestern Mali. The vertical wind shear is close to climatology during the afternoon and early evening before strengthening in the early morning hours when the convective activity occurs (Fig. 12b). This change is not found to be significant. Over this 24-h period there is a steady and significant increase in the atmospheric moisture content as the precipitable water increases by over 5 mm compared to climatology by 09Z ( $t_0+21$  h). This increase corresponds to a 5 – 10% increase in precipitable water after 00Z ( $t_0+12$  h). Much of this increase in atmospheric moisture occurs between 825 and 500 hPa while the atmosphere is marginally drier near the surface (Fig. 12d).

Fig. 12e shows the corresponding time series of absolute wind convergence over the area. Before 00Z ( $t_0 + 12$  h) the increase in atmospheric moisture between 700 - 850 hPa is associated with a significant increase in wind convergence as there is anomalous westerly flow (Fig. 12a) over southwestern Mali. Above 700 hPa there is a brief period of wind divergence around 21Z ( $t_0 + 9$  h) associated with the difluence of the flow between the two cyclonic circulations. By 03Z ( $t_0 + 15$  h) the southern storm track low has moved westward, and the mid-level anomalous flow becomes more easterly over southwestern Mali as it now lies in the northern flank this low (not shown). Below 750 hPa there is strong wind convergence between 03Z ( $t_0 + 15$  h) -10Z ( $t_0 + 22$  h).

Fig. 13 shows this transition in the zonal flow more clearly as Fig. 13a shows the time series of the area-averaged vertical p-velocity and zonal wind over the southwestern Mali study region from the weighted climatology for reference, while Fig. 13b shows the same fields for the Type D composite. Prior to 22Z ( $t_{\theta}$  + 10 h) the anomalous mid-level westerly flow associated with the coastal cyclone indicates a weakening of the mid-level AEJ at 600 hPa over southwestern Mali by approximately 1 - 2 m s<sup>-1</sup>. After 22Z the AEJ intensifies eventually becoming stronger than climatology around 01Z ( $t_0 + 13$  h). This intensification of the AEJ is associated with the southern storm track low as this circulation feature's center is slightly south of the study region so as this feature moves closer overnight the anomalous flow shifts from northerly/northeasterly to easterly. When this occurs, it strengthens the mid-level easterly flow, rising vertical motions (Fig. 13b), and mid-level wind divergence over southwestern Mali by 03Z (Fig. 12e). Below 900 hPa the westerly zonal flow is enhanced compared to climatology beginning at 19Z ( $t_0 + 7$  h) and peaking in magnitude at 03Z ( $t_0 + 15$  h) at 6 m s<sup>-1</sup>. This enhanced westerly low-level flow is associated with increased inflow into the approaching southern storm track cyclone, and by 03Z ( $t_0 + 15$  h) supports the strong low-level wind convergence into the developing storm system (Fig. 12e). Again, caution is required when interpreting these results as the fields as changes are not found to be statistically robust due in part to the small sample size of events.

Figures 14a and b show the 06Z ( $t_0 - 6$  h) Type D composite specific humidity and winds at 925 hPa and 800 hPa, respectively. The stippling denotes areas where the specific humidity difference from the weighted climatology is significant. At 925 hPa (Fig. 14a) there is strong low-level southwesterly flow that extends from the Liberia/Seirra Leone coast inland over Mali and eastern Mauritania associated with the circulation around the coastal low. This enhanced southwesterly flow is associated with increasing the low-level moisture north of 15°N over the northern Sahel of Mauritania and Mali. Over southwestern Mali the specific humidity is greater than 14 g kg<sup>-1</sup>. At 800 hPa (Fig. 14b) the westerly/southwesterly flow only extends to about 14°N and is more westerly than southwesterly compared to 925 hPa. Still specific humidity remains high with values greater than 10 g kg<sup>-1</sup> extending to 18°N and much of the northern Sahel is significantly wetter than normal.

While the strongest southwesterly flow at 925 hPa has shifted west by 00Z (t<sub>0</sub> + 12 h) as the midlevel coastal low continues to move westward (Fig. 14c), it still reaches southwestern Mali. The low-level environment remains relatively moist with specific humidity values greater than 14 g kg<sup>-1</sup> over much of West Africa. At 800 hPa (Fig. 14d) the mid-level flow becomes northeasterly over southwestern Mali ahead of the approaching southern storm track AEW. However, this transition to a northeasterly flow does not dry out the mid-level environment due to the earlier build-up of moisture over the northern Sahel.

By 06Z ( $t_0 + 18$  h) the 925 hPa flow is westerly over southwestern Mali, directed towards the southern storm track low over western Burkina Faso (Fig. 14e). Again, the low-level environment remains relatively moist (> 14 g kg<sup>-1</sup>) when the strongest convective activity is occurring over the southern Mali. At 800 hPa the flow remains northeasterly over southwestern Mali (Fig. 14f). While there is some evidence of drier air at 800 hPa over northern and central Mali, it has not yet reached southwestern Mali as specific humidity values remain greater than 10 g kg<sup>-1</sup>.

The atmospheric instability associated with the Type D event was also examined, but it is not found to be particularly strong. Fig. 15 shows Type D time series of composite mean CAPE (Fig. 15a) and CIN (Fig. 15b) area-averaged over the Mali analysis region. While CAPE is consistently 200 – 300 J kg<sup>-1</sup> lower than climatology over the period shown, this change is not significant. CIN is significantly lower in the early afternoon, late evening, and early morning hours, indicating a 35 – 45% reduction at these times. Maximum CAPE values never exceed 2000 J kg<sup>-1</sup> indicative of only marginal to moderate instability. There is also no temperature inversion cap over southwestern Mali and CIN values are lower than normal, especially in the early evening and overnight.

Thus, the Type D extreme rainfall event is associated with the passage of two successive AEWs. The circulation associated with the leading low is associated with reducing the mid-level easterly outflow of moisture out of the southern Sahel above 850 hPa (Fig. 12d) while increasing the atmospheric moisture content over the northern Sahel and southern Sahara (Figs. 14a & b). The approach of the second AEW in the early morning helps trigger the extreme convection over southwestern Mali by dynamically enhancing the low-level convergence in the significantly moist environment (Fig. 12). The exact timing of the

convective activity during the early morning (Fig. 12b) is dependent on the timing/location of the second approaching AEW. In contrast the Type A coastal low event is associated with a mid-latitude trough that extends southward into the subtropics. This means that Type A events are not dependent upon a second AEW approaching from the east to help dynamically force the convection, which was the case for Type D. Rather it is the vertical mixing of moist air upward driven by the daytime heating combined with reduced mid-level moisture transport out of the region due to the mid-level trough's presence that are most important for Type A.

### 5. Conclusions

NASA IMERG satellite-derived rainfall estimates and ERA5 atmospheric reanalysis data are analyzed to understand how boreal summer extreme rainfall forms over the southwestern Mali of the West African Sahel (8.05°W – 5.05°W; 12.05°N – 14.05°N). This area is observed to have more extreme 24-h rainfall events in boreal summer than other regions of the West African Sahel from 2000-2019 (VC22). Here we examine 24 extreme events identified by VC22 to identify common environmental factors associated with their development to aid in their prediction and explain why this region is favorable for extreme rainfall.

Events are sorted based on the timing of their peak rainfall rate - before 00Z for "PM events" or after 00Z for "AM events" - and associated mid-tropospheric synoptic patterns - a coastal ridge or a low between 15°N - 20°N preceding maximum rainfall - yielding four composite types. They are PM coastal low (Type A; 5 events), PM coastal ridging (Type B; 6 events), AM coastal ridging (Type C; 4 events), and AM coastal low (Type D; 7 events). 2 events did not fit any of these types and are not evaluated further. Of interest here is how both nearby coastal ridging and coastal troughing can lead to extreme rainfall over southwestern Mali.

Based on the analysis the following conclusions can be drawn:

• Temperature inversion caps can contribute to the development of extreme rainfall over the southwestern Mali. This occurs when an anomalous ridge is present over the northwestern Sahel/Sahara (Type B

and C events). In the wake of this ridge the environment over the northwestern Sahara becomes warmer and drier, intensifying the Saharan thermal low in this region. Anomalously dry and warm air is advected by the mid-level flow equatorward over the central and southern Sahel, producing a strong capping inversion that can inhibit the development of convection until the cap either dissipates or it is overcome by strong convection.

- behind the coastal ridge can be key for the development of extreme precipitation. Both Type B and C events have a mid-level low upstream over West Africa east of Mali (Figs. 2b c). Type B's low is an AEW at 10°N in the southern storm track, while Type C's low is the Saharan thermal low at 20°N. The low's location affects the extent to which the capping inversion can develop over southwestern Mali. When the low is in the southern storm track the capping inversion is weaker over southwestern Mali (Figs. 7b and 8b) allowing strong convection to develop in the afternoon for Type B. However, when the low is north of 20°N, it indicates a deepening of the Saharan thermal low and its circulation reinforces the equatorward advection of warm air over southwestern Mali yielding a strong capping inversion between 900 800 hPa (Fig. 10g) that inhibits the development of convective activity until the cap dissipates around 00Z.
- Coastal low extreme rainfall event types (Types A and D) significantly influence the mid-level but not the low level (e.g., below 850 hPa) moisture content over southwestern Mali (Figs. 3d and 12d). Intuitively one may expect these event types to be associated with enhanced inflow of moisture via the WAWJ since the coastal low strengthens the low-level westerly/southwesterly flow from the tropical Atlantic. While there is evidence of a stronger WAWJ (Figs. 5 and 13) there is not an increase in low-level moisture over southwestern Mali. Instead, this enhanced inflow is incorporated into the coastal low's eastern flank and directed northward into the northern Sahel and southern Sahara. Thus, there is no evidence of a low-level moisture plume being directly associated with these extreme rainfall event types for this region. Rather, the coastal low weakens the prevailing mid-level easterly flow between 10°N 15°N and thereby reduces the mid-level moisture transport out of southwestern Mali.

It is also important to consider approaching synoptic systems from the east for the coastal low extreme rainfall event types. Type D is associated with a second low, an AEW in the southern storm track (Fig. 2d), and Type A is not (Fig. 2a). While both types are associated with a significant increase in the atmospheric moisture content over the northern Sahel/southern Sahara of Mauritania and northern Mali (Figs. 4 & 14), it is the second low's circulation that transports some of the anomalous mid-level northern Sahel moisture southward (Fig. 14) and significantly increases the precipitable water (Fig. 12c) over southwestern Mali. Furthermore, wind convergence increases over southwestern Mali (Fig. 12e) as anomalous easterly flow associated with the northern flank of the second low convergences with anomalous westerly flow associated with the southern flank of the coastal low providing the strong dynamical forcing to the region. The absence of the second low is associated with weaker loading of moisture in the atmospheric column (Fig. 3c) and weaker wind convergence over southwestern Mali for the Type A events.

In summary, the location of southwestern Mali is key to making this area favorable for boreal summer convective activity including extreme rainfall events. The area is relatively close to the Atlantic Ocean (~700 km) which is an important source of moisture for summer convective activity over West Africa (Cook 1997; Thorncroft et al. 2011; Pu and Cook 2010, 2012). The region also lies about 1000 km south of the Sahara Desert where the Saharan thermal low forms due to strong boreal summer heating (Knippertz and Fink 2008; Lavaysse et al. 2009). While the thermal low's location is relatively stationary during boreal summer, positioned just east/southeast of the Hoggar Mountains (Lavaysse et al. 2009), it varies in intensity on different timescales and influences the regional circulation and moisture transport over West Africa (Mathon et al. 2002; Fink and Reiner 2003; Parker et al. 2005; Lavaysse et al. 2010a, 2010b, 2013) as well as the strength and longevity of the temperature inversion cap over southwestern Mali as shown by this study. Additionally, southwestern Mali (12°N - 15°N) lies within the boreal summer southern storm track of AEW disturbances (Diehiou et al. 1999; Fink and Reiner 2003; Hsieh and Cook 2005, 2008). AEW disturbances are conducive to MCS development over West Africa (Carlson 1969a,b; Reed et al. 1977) and in some instances extreme rainfall events (Engel et al. 2017; Fall et al. 2020; Vizy and Cook 2022;

Chahinian et al. 2023). This region is favorable for convective development including extreme rainfall due to how all these above-mentioned factors interact to influence the regional circulation, moisture transport, and instability over southwestern Mali under the specific synoptic conditions discussed in this study (Fig. 2).

This study provides a good start for understanding the circulation and environmental conditions associated with the development of these selected extreme rainfall events over southwestern Mali. That said, more work is needed to compare these features/conditions with other regions of West Africa to fully understand how they differ over southwestern Mali and lead to more frequent extreme rainfall events over this region. Furthermore, while the results presented here are encouraging in that they have identified common factors associated with extreme rainfall events examined over the southwestern Mali, there are still variations among the individual events that must be better understood in future work to be able to better predict their timing and location. This includes examining a larger population of events as this study focused only on the most extreme rainfall-producing events. Doing so would improve our assessment of the statistical robustness of the mechanisms/processes identified here, especially for processes associated with fields that are inherently highly variable such as vertical motion, wind convergence, and precipitation. Additionally, more work is still needed to validate the selection approach used by this study. With the knowledge gained from this study a more objective classification approach could be devised to confirm the findings for the different composite types and the importance of the diurnal timing of the rainfall. Likewise, further work is needed to confirm the relative roles in coastal ridging and coastal troughing in producing heavy rainfall over southwestern Mali and western West Africa in general. Finally, the extent to which the relatively moist Niger River delta may be contributing moisture also needs to be examined.

**Acknowledgements:** This work was funded by NSF Award #1929074. The authors acknowledge the Texas Advanced Computing Center (TACC) at The University of Texas at Austin for providing HPC and database resources that have contributed to the research results reported within this paper. URL: <a href="http://www.tacc.utexas.edu">http://www.tacc.utexas.edu</a>.

#### References

- Anash SO, Ahiatahu MA, Yorke CK, Out-Larbi F, Yahaya B, Lamptey PNL, Tanu M (2020)

  Meteorological analysis of floods in Ghana. Advances in Meteorol 4230627: 1 14.

  <a href="https://doi.org/10.1155/2020/4230627">https://doi.org/10.1155/2020/4230627</a>
- Burpee RW (1972) The origin and structure of easterly waves in the lower troposphere of North Africa. J Atmos Sci 29: 77-90. https://doi.org/10.1175/1520-0469(1972)029<0077:TOASOE>2.0.CO;2
- Carlson TN (1969a) Synoptic histories of three African disturbances that developed into Atlantic hurricanes. Mon Wea Rev 97: 256-276. <a href="https://doi.org/10.1175/1520-0493(1969)097,0256:SHOTAD.2.3.CO;2">https://doi.org/10.1175/1520-0493(1969)097,0256:SHOTAD.2.3.CO;2</a>
- Carlson TN (1969b) Some remarks on African disturbances and their progress over the tropical Atlantic.

  Mon Wea Rev 97: 716–726. <a href="https://doi.org/10.1175/1520-0493(1969)097<0716:SROADA>2.3.CO;2">https://doi.org/10.1175/1520-0493(1969)097<0716:SROADA>2.3.CO;2</a>
- Chagnaud G, Panthou G, Vischel T, Lebel T (2022) A synthetic view of rainfall intensification in the West African Sahel. Environ Res Lett 17: 044005. <a href="https://doi.org/10.1088/1748-9326/ac4a9c">https://doi.org/10.1088/1748-9326/ac4a9c</a>
- Chahinian N, Alcoba M, Dembélé NDJ, Cazenave F, Bouvier C (2023) Evaluation of an early flood warning system in Bamako (Mali): Lessons learned from the flood of May 2019. J Flood Risk Management.

  16: e12878. <a href="https://doi.org/10.1111/jfr3.12878">https://doi.org/10.1111/jfr3.12878</a>
- Cook KH (1997) Large-scale atmospheric dynamics and Sahelian precipitation. J Climate 10: 1137-1152. https://doi.org/10.1175/1520-0442(1997)010<1137:LSADAS>2.0.CO;2
- Cook KH (1999) Generation of the African easterly jet and its role in determining West African precipitation. J Clim 12: 1165-1184. <a href="https://doi.org/10.1175/1520-0442(1990)012<1165:GOTAEJ>2.0.CO;2">https://doi.org/10.1175/1520-0442(1990)012<1165:GOTAEJ>2.0.CO;2</a>
- Cook KH (2015) Role of intertial instability in the West African monsoon jump. J Geophys Res Atmos 120: 3085-3102. <a href="https://doi.org/10.1002/2014JD022579">https://doi.org/10.1002/2014JD022579</a>

- Cornforth RJ, Mumba Z, Parker DJ, et al (2017) Synoptic systems. Meteorology of Tropical West Africa:

  The Forecasters' Handbook, D. J. Parker and M. Diop-Kane, Eds., Wiley-Blackwell, 40–89,

  <a href="https://doi.org/10.1002/9781118391297.ch2">https://doi.org/10.1002/9781118391297.ch2</a>
- Cuesta J, Marsham JH, Parker DJ, Flamant C (2009) Dynamical mechanisms controlling the vertical redistribution of dust and the thermodynamic structure of the West African atmospheric boundary layer during summer. Atmos Sci Let 10: 34-42. https://doi.org/10.1002/asl.207
- Danso DK, Anquetin S, Diedhiou A, Lavaysse C, Kobea A, Touré NE (2019) Spatio-temporal variability of cloud cover types in West Africa with satellite-based and reanalysis data. Q J Roy Meteorol Soc 145: 3715-3731. <a href="https://doi.org/10.1002/qj.3651">https://doi.org/10.1002/qj.3651</a>
- Di-Baldassarre G, Montanari A, Lins H, Koutsoyiannis D, Brandimarte L, Blöschl G (2010) Flood fatalities in Africa: From diagnosis to mitigation. Geophys Res Lett 37: 1 5. https://doi.org/10.1029/2010GL045467
- Diehiou A, Janicot S, Viltard A, de Felice P, Laurent H (1999) Easterly wave regimes and associated convection over West Africa and tropical Atlantic: Results from the NCEP/NCAR and ECMWF reanalyses. Clim Dyn 15: 795-822. <a href="https://doi.org/10.1007/s003820050316">https://doi.org/10.1007/s003820050316</a>
- Doswell CA III, Brooks HE, Maddox RA (1996) Flash flood forecasting: An ingredients-based methodology. Wea Forecasting 11: 560-581. <a href="https://doi.org/10.1175/1520-0434(1996)011<0560:FFFAIB>2.0.CO;2">https://doi.org/10.1175/1520-0434(1996)011<0560:FFFAIB>2.0.CO;2</a>
- Duvel J-P (1989) Convection over tropical Africa and the Atlantic Ocean during northern summer. Part I: Interannual and diurnal variations. Mon Wea Rev 117: 2782–2799. <a href="https://doi.org/10.1175/1520-0493(1989)117<2782:COTAAT>2.0.CO;2">https://doi.org/10.1175/1520-0493(1989)117<2782:COTAAT>2.0.CO;2</a>
- Egbinola CN, Olaniran HD, Amanambu AC (2017) Flood management in cities of developing countries:

  The example of Ibadan, Nigeria. Journal of Flood Risk Management 10: 546–554.

  <a href="https://doi.org/10.1111/jfr3.12157">https://doi.org/10.1111/jfr3.12157</a>

- Elagib NA, Zayed ISA, Saad SAG, Mahmood MI, Basheer M, Fink AH (2021) Debilitating floods in the Sahel are becoming frequent. J Hydrology 599: 126362. <a href="https://doi.org/10.1016/j.jhydrol.2021.126362">https://doi.org/10.1016/j.jhydrol.2021.126362</a>
- Eldridge RH (1957) A synoptic study of West African disturbance lines. Q J Roy Meteorol Soc 83: 303 314. <a href="https://doi.org/10.1002/qj.49708335704">https://doi.org/10.1002/qj.49708335704</a>
- Engel T, Fink AH, Knippertz P, Pante G (2017) Extreme precipitation in the West African cities of Dakar and Ouagadougou: Atmospheric dynamics and implications for flood risk assessments. J Hydrometeorol 18: 2937-2957. https://doi.org/10.1175/JHM-D-16-0218.1
- Engelstaedter S, Washington R, Flamant C, Parker DJ, Allen CJT, Todd MC (2015) The Saharan heat low and moisture transport pathways in the central Sahara Multiaircraft observations and African-LAM evaluation. J Geophys Res Atmos 120: 4417-4442. https://doi.org/10.1002/2015JD023123
- Fall M, Dieng AL, Sall SM, Sane Y, Diakhaté (2020) Synoptic analysis of extreme rainfall event in West

  Africa: The case of Linguère. American J of Environmental Protection 8: 1-9.

  <a href="https://doi.org/10.12691/env-8-1-1">https://doi.org/10.12691/env-8-1-1</a>
- Fink AH, Reiner A (2003) Spatiotemporal variability of the relation between African easterly waves and West African squall lines in 1998 and 1999. J Geophys Res 108: 4332. https://doi.org/10.1029/2002JD002816
- Fitzpatrick RGJ, Parker DJ, Marsham JH, Rowell DP, and co-authors (2020) What drives the intensification of mesoscale convective systems over the West African Sahel under climate change? J Climate 33: 3151-3172. <a href="https://doi.org/10.1175/JCLID-19-0380.1">https://doi.org/10.1175/JCLID-19-0380.1</a>
- Fofana M, Adounkpe J, Larbi I, and co-authors (2022) Urban flash flood and extreme rainfall events trend analysis in Bamako, Mali. Environmental Challenges 6: 100449.

  <a href="https://doi.org/10.1016/j.envc.2022.100449">https://doi.org/10.1016/j.envc.2022.100449</a>
- Galvin JFP (2010) Two easterly waves in West Africa in summer of 2009. Weather 65: 219-227. https://doi.org/10.1002/wea.605

- Grodsky SA, Carton JA, Nigam S (2003) Near surface westerly wind jet in the Atlantic ITCZ. Geophys Res Lett 30: 2009. https://doi.org/10.1029/2003GL017867
- Han F, Cook KH, Vizy EK (2019) Changes in intense rainfall events and drought across Africa in the 21<sup>st</sup> century. Clim Dyn 53: 2757-2777. https://doi.org/10.1007/s00382-019-04653-z
- Hersbach H, Bell B, Berrisford P, Hirahara S, and co-authors (2020) The ERA5 global reanalysis. Q J Roy Meteorol Soc 146: 1999-2049. https://doi.org/10.1002/qj.3803
- Hsieh J-S., Cook KH (2005) Generation of African easterly wave disturbances: Relationship to the African easterly jet. Mon Wea Rev 133: 1311-1327. https://doi.org/10.1175/MWR2916.1
- Hsieh J-S., Cook KH (2008) On the instability of the African easterly jet and the generation of African waves: Reversals of the potential vorticity gradient. J Atmos Sci 65: 2130-2151. https://doi.org/10.1175/2007JAS2552.1
- Huffman GJ, Bolvin DT, Braithwaite D, Hsu K, Joyce R, Kidd C, Nelkin EJ, Sorooshian S, Tran J, Xie P (2020) NASA Global Precipitation Measurement (GPM) Integrated Multi-satellitE Retrievals for GPM (IMERG). Algorithm Theoretical Basis Doc., version 6.3, 30 pp., https://gpm.nasa.gov/sites/default/files/2020-05/IMERG ATBD V06.3.pdf
- Kendon EJ, Stratton RA, Tucker S, Marsham JH, Berthou S, Rowell DP, Senior CA (2019) Enhanced future changes in wet and dry extremes over Africa and convection-permitting scale. Nat Commun 10: 1794. https://doi.org/10.1038/s41467-019-09776-9
- Klein C, Nkrumah F, Taylor CM, Adefisan EA (2021) Seasonality and trends of drivers of mesoscale convective systems in southern West Africa. J Climate 34: 71 87. <a href="https://doi.org/10.1175/JCLI-D-20-0194.1">https://doi.org/10.1175/JCLI-D-20-0194.1</a>
- Knippertz P, Fink A (2008) Dry-season precipitation in tropical West Africa and its relation to forcing from the extratropics. Mon Wea Rev 136: 3579-3596. https://doi.org/10.1175/2008MWR2295.1
- Knippertz P, Martin JE (2005) Tropical plumes and extreme precipitation in subtropical and tropical West Africa. Q J R Meteorol Soc 131: 2337-2365. <a href="https://doi.org/10.1256/qj.04.148">https://doi.org/10.1256/qj.04.148</a>

- Lafore JP, Beucher F, Peyrillé and co-authors (2017a) A multi-scale analysis of the extreme rain event of Ouagadougou in 2009. Q J Roy Meteorol Soc 143: 3094-3109. https://doi.org/10.1002/qj.3165
- Lafore, JP, Chapelon N, Beucher F, and co-authors (2017b) West African synthetic analysis and forecast:

  WASA/F. In: D.J. Parker and J. Diop-Kane (Eds.) Meteorology of Tropical West Africa.

  Chichester, UK: Wiley Blackwell, pp. 423–451. <a href="https://doi.org/10.1002/9781118391297.ch11">https://doi.org/10.1002/9781118391297.ch11</a>
- Laing AG, Carbone R, Levizzani V, Tuttle J (2008) The propagation and diurnal cycles of deep convection in northern tropical Africa. Quart J Roy Meteorol Soc 134: 93–109. https://doi.org/10.1002/qj.194
- Lavaysse C, Flamant C, Janicot S, Parker DJ, Lafore J-P, Sultan B, Pelon J (2009) Seasonal evolution of the West African heat low: A climatological perspective. Clim Dyn 33: 313-330. https://doi.org/10.1007/s00382-009-0553-4
- Lavaysse C, Flamant C, Janicot S (2010a) Regional-scale convection patterns during strong and weak phases of the Saharan heat low. Atmos Sci Let 11: 255-264. https://doi.org/10.1002/asl.284
- Lavaysse C, Flamant C, Janicot S, Knippertz P (2010b) Links between the African easterly waves, midlatitude circulation and intraseasonal pulsations of the West African heat low. Q J R Meteorol Soc 136: 141-158. <a href="https://doi.org/10.1002/qj.555">https://doi.org/10.1002/qj.555</a>
- Lavaysse C, Eymard L, Flamant C, Karbou F, Mimouni M, Saci A (2013) Monitoring the West African heat low at seasonal and intra-seasonal timescales using AMSU-A sounder. Atmos Sci Let 14: 263-271. <a href="https://doi.org/10.1002/asl2.449">https://doi.org/10.1002/asl2.449</a>
- Lélé MI, Lamb PJ (2010) Variability of the Intertropical front (ITF) and rainfall over the West African Sudan-Sahel zone. J Climate 23:3984-4004. <a href="https://doi.org/10.1175/2010JCLI3277.1">https://doi.org/10.1175/2010JCLI3277.1</a>
- Li F, Chavas DR, Reed KA, Dawson II DT (2020) Climatology of severe local storm environments and synoptic-scale features over North America in ERA5 reanalysis and CAM6 simulation. J Climate, <a href="https://doi.org/10.1175/JCLI-D-19-0986.1">https://doi.org/10.1175/JCLI-D-19-0986.1</a>
- Liu W, Cook KH, Vizy EK (2020) Role of the West African westerly jet in the seasonal and diurnal cycles of precipitation over West Africa. Clim Dyn 54: 843-861. <a href="https://doi.org/10.1007/s00382-019-05035-1">https://doi.org/10.1007/s00382-019-05035-1</a>

- Mahmood MI, Elagib NA, Horn F, Saad SAG (2017) Lessons learned from Khartoum flash flood impacts:

  An integratedassessment. Science of the Total Environment 601–602: 1031–1045.

  https://doi.org/10.1016/j.scitotenv.2017.05.260
- Marsham JH, Dixon N, Garcia-Carreras L, Lister G, Parker DJ, Knippertz P, Birch C (2013) The role of moist convection in the West African monsoon system—insights from continental-scale convection-permitting simulations. Geophys Res Lett 40: 1843–1849.

  <a href="https://doi.org/10.1002/grl.50347">https://doi.org/10.1002/grl.50347</a>
- Mathon V, Laurent H, Lebel T (2002) Mesoscale convective system rainfall in the Sahel. J Appl Meteorol 41: 1081–1092. https://doi.org/10.1175/1520-0450(2002)041<1081:MCSRIT>2.0.CO;2
- Miller J, Taylor C, Guicard F, and co-authors (2022) High-impact weather and urban flooding in the West

  African Sahel A multidisciplinary case study of the 2009 event in Ouagadougou. Weather and

  Climate Extremes 36: 100462. <a href="https://doi.org/10.1016/j.wace.100462">https://doi.org/10.1016/j.wace.100462</a>
- Mohr KI, Thorncroft CD (2006) Intense convective systems in West Africa and their relationship to the African easterly jet. Q J Roy Meteorol Soc 132: 163–176. https://doi.org/10.1256/qj.05.55
- Panthou G, Vischel T, Lebel T (2014) Short Communication: Recent trends in the regime of extreme rainfall in the Central Sahel. Int J Climatol 34: 3998-4006. <a href="https://doi.org/10.1002/joc.3984">https://doi.org/10.1002/joc.3984</a>
- Parker DJ, Burton RR, Diongue-Niang A, Ellis RJ, Felton M, Taylor CM, Thorncroft CD, Bessemoulin P, Tompkins AM (2005) The diurnal cycle of the West African monsoon circulation. Quart J Roy Meteorol Soc 131: 2839–2860. <a href="https://doi.org/10.1256/qj.04.52">https://doi.org/10.1256/qj.04.52</a>
- Peters M. Tetzlaff G (1988) The structure of West African squall lines and their environmental moisture budget. Meteorol Atmos Phys 39: 74 84. <a href="https://doi.org/doi:10.1007/BF01041933">https://doi.org/doi:10.1007/BF01041933</a>
- Provod M, Marsham JH, Parker DJ, Birch CE (2016) A characterization of cold pools in the West African Sahel. Mon Weather Rev 144: 1924–1934. <a href="https://doi.org/10.1175/MWR-D-15-0023.1">https://doi.org/10.1175/MWR-D-15-0023.1</a>
- Pu B, Cook KH (2010) Dynamics of the West African westerly jet. J Clim 23: 6263 6276. https://doi.org/10.1175/2010JCLI3648.1

- Pu B, Cook KH (2012) Role of the West African westerly jet in Sahel rainfall variations. J Clim 25: 5748-5767. https://doi.org/10.1175/JCLI-D-11-00394.1
- Redelsperger JL, Lafore JP (1988) A three-dimensional simulation of a tropical squall-line: convective organization and thermodynamic vertical transport. J Atmos Sci 45:1334–1356. https://doi.org/10.1175/1520-0469(1988)045<1334:ATDSOA>2.0.CO;2
- Reed RJ, Norquist DC, Recker EE (1977) The structure and properties of African wave disturbances as observed during Phase III of GATE. Mon Wea Rev 105: 317-333. <a href="https://doi.org/10.1175/1520-0493(1977)105<0317:TSAPOA>2.0.CO;2">https://doi.org/10.1175/1520-0493(1977)105<0317:TSAPOA>2.0.CO;2</a>
- Rowell DP, Milford JR (1993) On the generation of African squall lines. J Clim 6: 1181-1193. https://doi.org/10.1175/1520-0442(1993)006<1181:OTGOAS>2.0.CO;2
- Saley LA, Salack S (2023) Present and future of heavy rain events in the Sahel and West Africa. Atmosphere 14: 965. <a href="https://doi.org/10.3390/atmos14060965">https://doi.org/10.3390/atmos14060965</a>
- Sougué M, Merz B, Sogbedji JM, Zougmoré (2023) Extreme rainfall in southern Burkina Faso, West Africa:

  Trends and links to Atlantic sea surface temperature. Atmosphere 14: 284.

  <a href="https://doi.org/10.3390/atmos14020284">https://doi.org/10.3390/atmos14020284</a>
- Taylor CM, Belušić D, Guichard F, Parker DJ, Vischel T, Brock O, Harris PP, Janicot S, Klien C, Panthou G (2017) Frequency of extreme Sahelian storms tripled since 1982 in satellite observations. Nature 544: 475-478. <a href="https://doi.org/10.1038/nature22069">https://doi.org/10.1038/nature22069</a>
- Tetzlaff G, Peters M (1988) A composite study of early summer squall lines and their environment over West Africa. Meteorol Atmos Phys 38: 153–163. https://doi.org/10.1007/BF01029779
- Thorncroft CD, Blackburn M (1999) Maintenance of the African easterly jet. Quart J Roy Meteor Soc 125: 763-786. https://doi.org/10.1002/qj.49712555502
- Thorncroft CD, Nguyen H, Zhang C (2011) Annual cycle of the West African monsoon: Regional circulations and associated water vapour transport. Q J Roy Meteorol Soc 137: 129-147. https://doi.org/10.1002/qj.728

- Tramblay Y, Villarini G, Zhang W (2020) Observed changes in flood hazard in Africa. Environ Res Lett 15: 1040b5. https://doi.org/10.1088/1748-9326/abb90b
- Tschakert P, Sagoe R, Ofori-Darko G, Codjoe SN (2010) Floods in the Sahel: An analysis of anomalies, memory, and anticipatory learning. Climatic Change 103: 471-502. https://doi.org/10.1007/s10584-009-9776-y
- United Nations (2022). "2022 Revision of World Population Prospects". United Nations.

  <a href="https://population.un.org/wpp/Download/Files/1\_Indicators%20(Standard)/EXCEL\_FILES/1\_General/WPP2022\_GEN\_F01\_DEMOGRAPHIC\_INDICATORS\_COMPACT\_REV1.xlsx">Indicators%20(Standard)/EXCEL\_FILES/1\_General/WPP2022\_GEN\_F01\_DEMOGRAPHIC\_INDICATORS\_COMPACT\_REV1.xlsx</a>.

  Accessed 10/16/2023.
- Vizy EK, Cook KH (2009) A mechanism for African monsoon breaks: Mediterranean cold air surges. J Geophys Res 114: D01104. https://doi.org/10.1029/2008JD010654
- Vizy EK, Cook KH (2018) Mesoscale convective systems and nocturnal rainfall over the West African Sahel: Role of the Inter-tropical front. Clim Dyn 50: 587-614. <a href="https://doi.org/10.1007/s00382-017-3628-7">https://doi.org/10.1007/s00382-017-3628-7</a>
- Vizy EK, Cook KH (2019) Observed relationship between the Turkana low-level jet and boreal summer convection. Clim. Dyn 53: 4037 4058. https://doi.org/10.1007/s00382-019-04769-2
- Vizy EK, Cook KH (2022) Distribution of extreme rainfall events and their environmental controls in the West African Sahel and Soudan. Clim. Dyn 59: 997 1026. <a href="https://doi.or/10.1007/s00382-022-06171-x">https://doi.or/10.1007/s00382-022-06171-x</a>
- Vizy EK, Cook KH (2023) West African Sahel extreme rainfall events: Understanding storm development over the Damergou Gap using WRF convection-permitting simulations. *QJRoy Meteorol Soc* 149: 959 983. <a href="https://doi.org/10.1002/qj.4443">https://doi.org/10.1002/qj.4443</a>
- Zhang G, Cook KH (2014) West African monsoon demise: Climatology, interannual variations, and relationship to seasonal rainfall. J Geophys Res Atmos 119: 10175-10193. <a href="https://doi.org/10.1002/2014JD022043">https://doi.org/10.1002/2014JD022043</a>

#### **Statements and Declarations:**

**Funding:** This work was funded by NSF Award #1929074

**Competing Interests:** The authors have no relevant financial or non-financial interests to disclose.

**Author Contributions:** All authors contributed to the study conception and design. Material preparation and analysis were performed by E.K. Vizy. The manuscript was written by E.K. Vizy with feedback from K.H. Cook. All authors read and approve the final manuscript.

Data Availability: All datasets analyzed in this study are freely available from their original sources.

NASA IMERG final run satellite-derived rainfall data is available from NASA at

<a href="https://gpm.nasa.gov/data/directory">https://gpm.nasa.gov/data/directory</a>. ERA5 reanalysis is available from the Copernicus Climate Data

Store at <a href="https://cds.climate.copernicus.eu/cdsapp#!/dataset/reanalysis-era5-pressure-levels?tab=form">https://cds.climate.copernicus.eu/cdsapp#!/dataset/reanalysis-era5-pressure-levels?tab=form</a>

Table 1. Top 100 Southwestern Mali extreme rainfall events identified by  $VC22^*$ 

				Total	Hour	Max		
		Lon	Lat	Rainfall	Max	Intensity	Duration	Class
Event	Date	(°E)	(°N)	(mm)	Rate (Z)	(mm/d)	(hrs)	Type
1	05-06 JUL 2001	-7.55	12.95	145.2	19:30	1126	12.5	Type A
2	13-14 JUL 2006	-7.05	13.15	172.2	22:30	954	8.5	Type A
3	24-25 JUL 2003	-7.95	12.75	178.5	18:30	1425	9.5	Type B
4	02-03 AUG 2005	-7.75	12.05	169.8	22:30	1458	7.5	Type B
5	04-05 AUG 2011	-7.85	14.45	161.5	21:30	1452	8.0	Type B
6	07-08 AUG 2012	-6.35	12.55	280.8	14:00	1264	19.5	Type B
7	20-21 AUG 2004	-7.95	14.45	148.6	19:00	1673	8.0	Type B
8	22-23 AUG 2012	-7.75	12.35	149.1	13:30	1817	7.5	Type A
9	23-24 AUG 2011	-7.35	12.85	143.6	14:00	1469	5.0	Type A
10	26-27 AUG 2005	-7.25	13.55	188.2	15:30	1858	13.0	Type B
11	03-04 SEP 2010	-7.95	13.65	197.2	18:00	1379	9.5	Type A
12	18-19 SEP 2010	-8.05	12.85	161.7	21:30	1338	14.0	-
13	30 SEP -01 OCT 2003	-7.85	12.35	147.7	22:30	1710	5.5	-
14	05-06 OCT 2002	-6.85	13.25	180.4	18:30	1719	13.0	-
15	08-09 OCT 2008	-7.85	12.95	145.9	22:30	1834	4.5	-
16	10-11 OCT 2008	-7.85	12.15	161.3	14:00	1776	5.0	-
17	31 MAY - 01 JUN 2010	-5.85	12.35	146.8	07:00	1791	9.0	-
18	12-13 JUL 2003	-7.55	13.25	187.9	02:30	1600	6.5	Type C
19	14-15 JUL 2007	-5.65	13.25	203.1	01:30	1140	15.5	Type C
20	19-20 JUL 2004	-7.75	12.55	197.7	02:00	1623	8.5	Type C
21	19-20 JUL 2010	-7.55	12.95	162.0	02:00	981	13.5	Type C
22	05-06 AUG 2019	-7.35	14.25	165.2	02:00	1243	12.0	-
23	14-15 AUG 2003	-7.35	12.55	167.8	01:30	1695	12.0	Type D
24	14-15 AUG 2010	-6.95	13.55	158.6	02:00	1220	9.5	Type D
25	18-19 AUG 2011	-6.55	14.05	167.5	06:30	891	8.5	Type D
26	23-24 AUG 2003	-7.55	12.25	165.3	03:00	1221	13.5	Type D
27	23-24 AUG 2019	-6.75	13.65	225.1	05:30	730	15.5	Type D
28	24-25 AUG 2011	-5.15	12.05	160.1	02:00	1061	12.0	-
29	25-26 AUG 2006	-8.05	14.65	157.3	08:30	1739	9.0	Type D
30	01-02 SEP 2009	-7.85	13.15	225.0	10:00	2202	12.0	Type D
31	19-20 OCT 2008	-7.65	12.45	164.7	02:00	1372	7.5	-

<sup>\*</sup> Italics indicate events that occurred outside the June 15 – September 15 boreal summer monsoon season and are excluded from analysis.

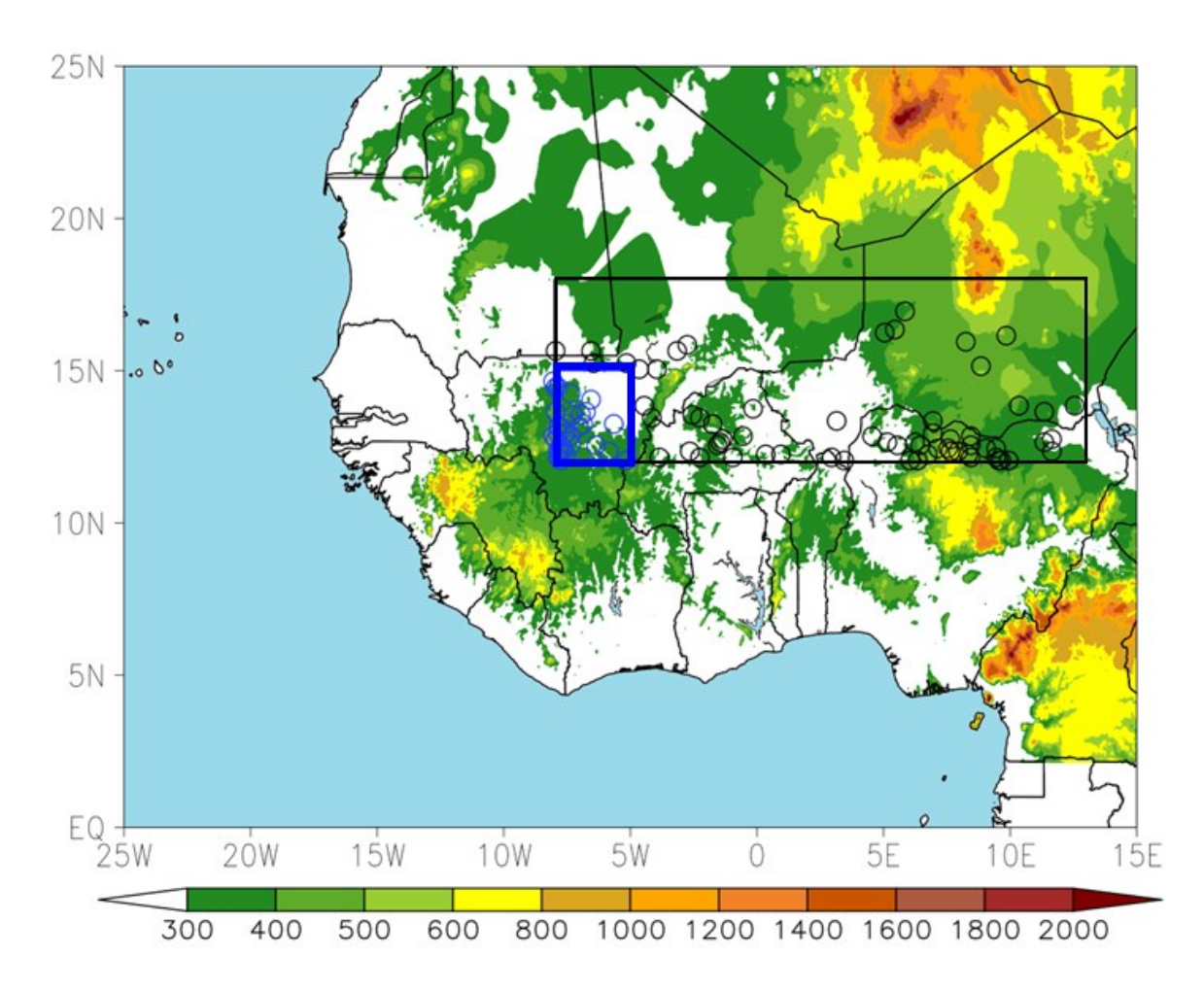


**Fig. 1** VC22's West African Sahel analysis region (black box) and the southwestern Mali region (blue box) along with the location of the top 100 24-h extreme rainfall events within (blue circles) and outside of (black circles) of the southwestern Mali area. Topography (shaded) is in meters.

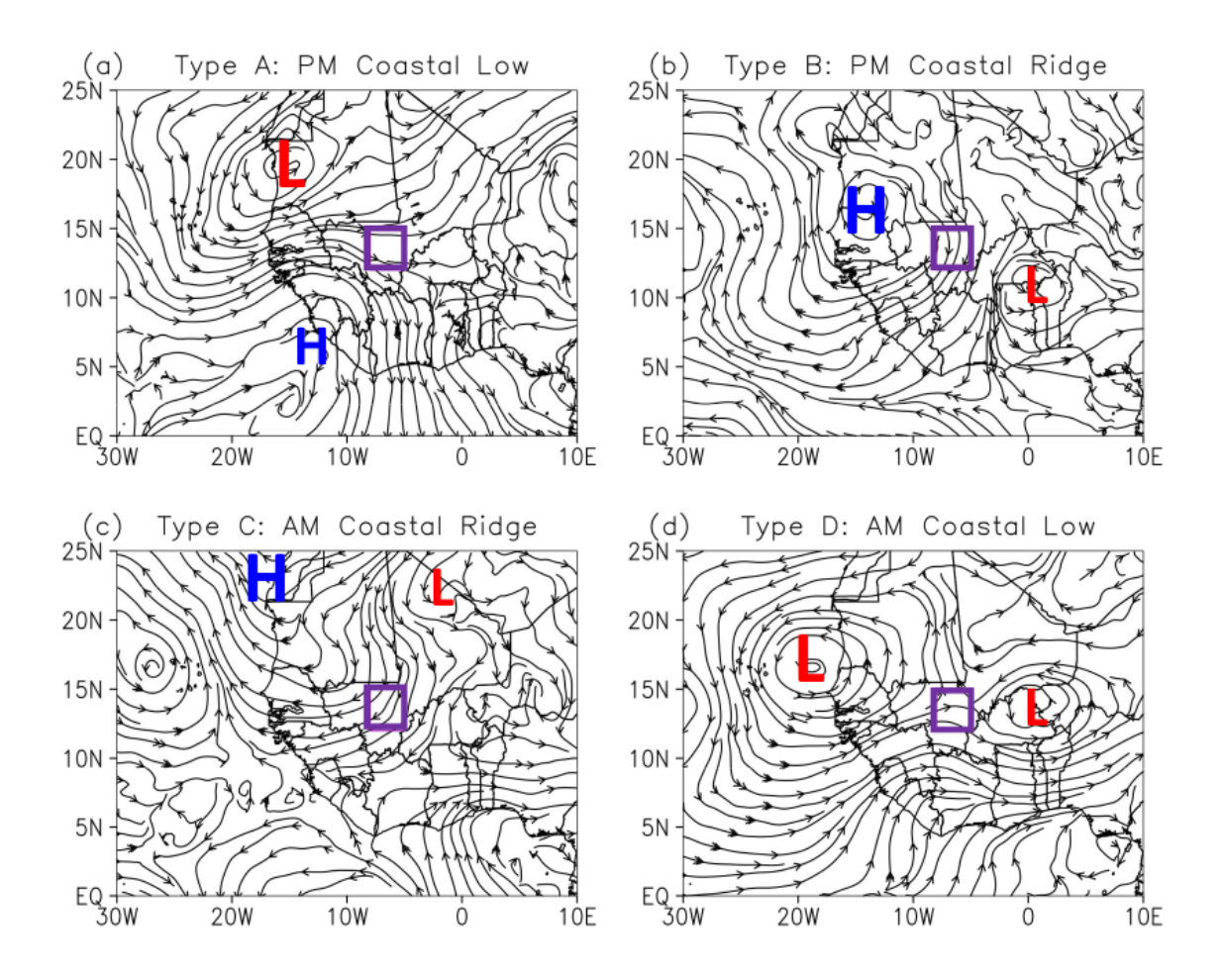


**Fig. 2** The 4 southwestern Mali boreal summer extreme rainfall events classification types as indicated by the 700 hPa streamline anomalies at 12Z ( $t_0$ ). The box indicates the Mali analysis region. Peak rainfall intensity at the maximum 12Z – 12Z 24-h total site occurs before (after) 00Z for the PM (AM) events.

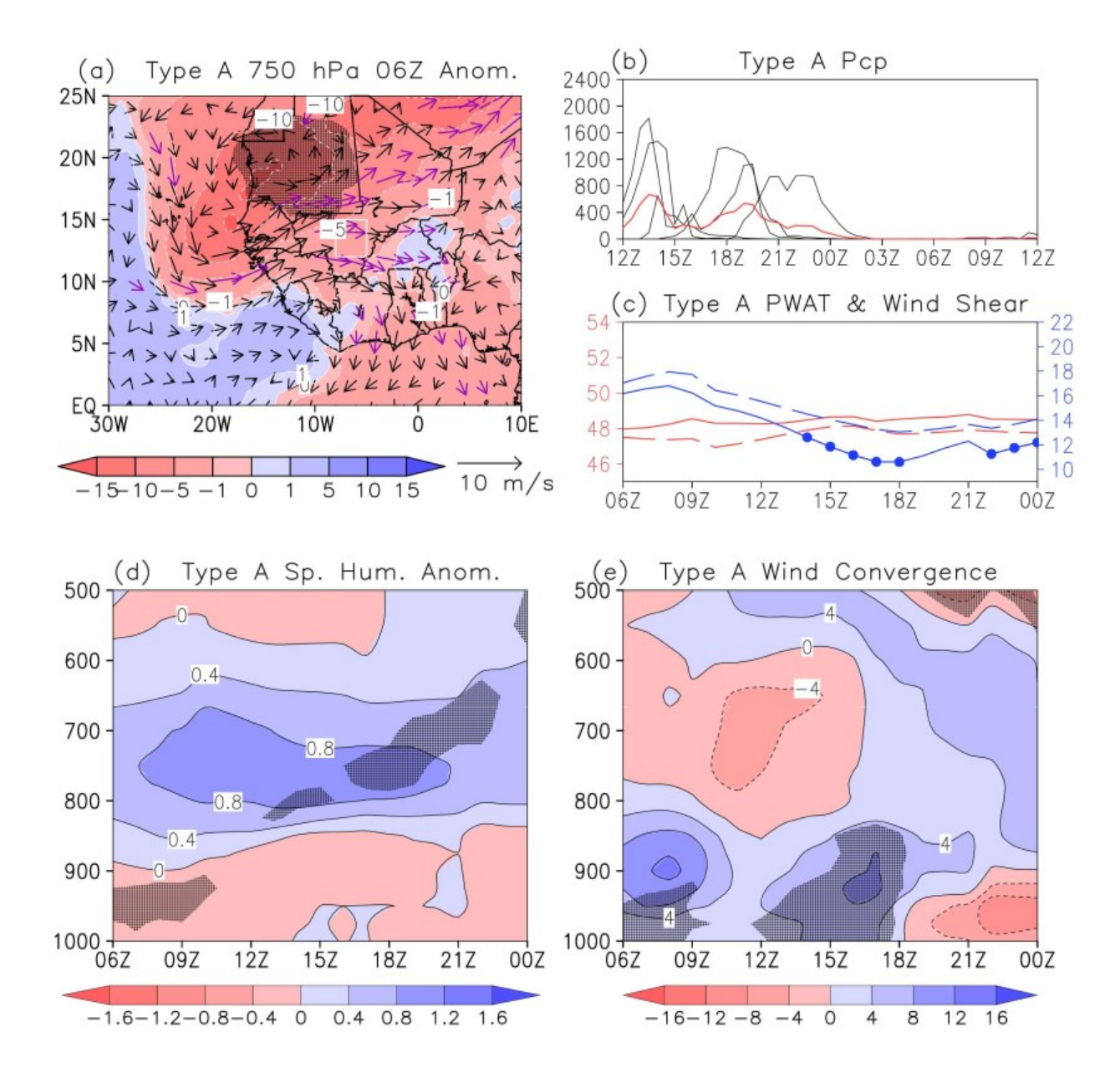


**Fig. 3** Type A **(a)** ERA5 06Z ( $t_0 - 6 h$ ) composite 750 hPa geopotential height (m) and wind (m s<sup>-1</sup>) anomalies. **(b)** IMERG rainfall rate (mm day<sup>-1</sup>) 12Z – 12Z time series for individual events at the maximum site locations (black lines) and the composite mean (red line). **(c)** ERA5 composite mean (solid lines) and the climatological (dashed lines) area-averaged precipitable water (red; mm) and 600 hPa – 925 hPa wind shear (m s<sup>-1</sup>; blue) time series over the Mali analysis region. Vertical profile time series of ERA5 area-averaged **(d)** specific humidity anomalies (g kg<sup>-1</sup>) and **(e)** absolute wind convergence (x10<sup>-6</sup> s<sup>-1</sup>) over the Mali analysis region. Hatching/dots/purple wind vectors denote significant differences from the weighted climatology at the 90% level of confidence using a student's t-test.

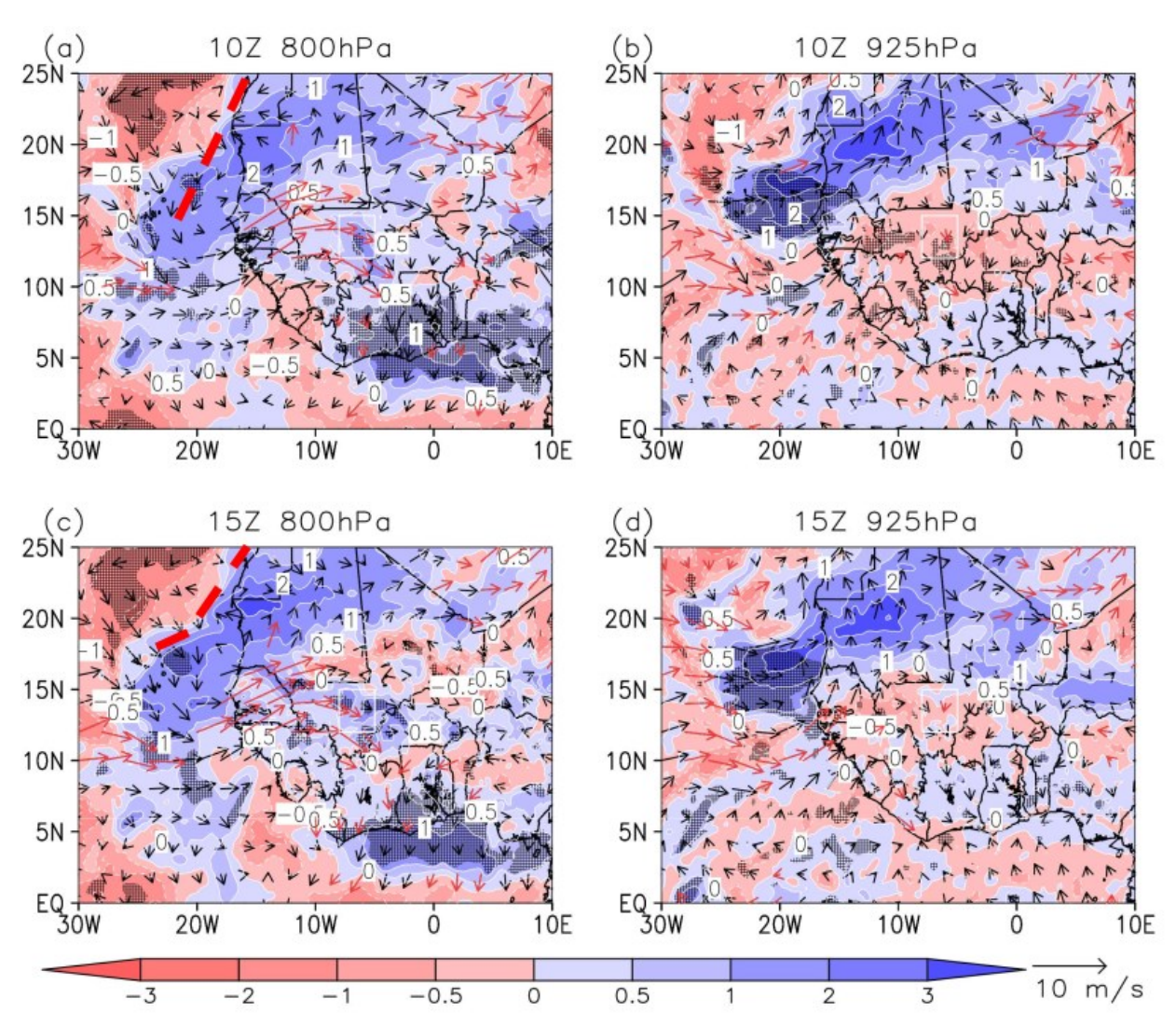


**Fig. 4** ERA5 Type A  $10Z(t_0 - 2h)$  specific humidity (shaded; g kg<sup>-1</sup>) and wind (vectors; m s<sup>-1</sup>) at **(a)** 800 hPa and **(b)** 925 hPa. **(c)** and **(d)** are the same as (a) and (b) but for  $15Z(t_0 + 3h)$ . Hatching/red vectors denote anomalies significant at the 90% level of confidence. White box denotes the Mali analysis region. Red dashed lines denote the mid-level coastal trough position.

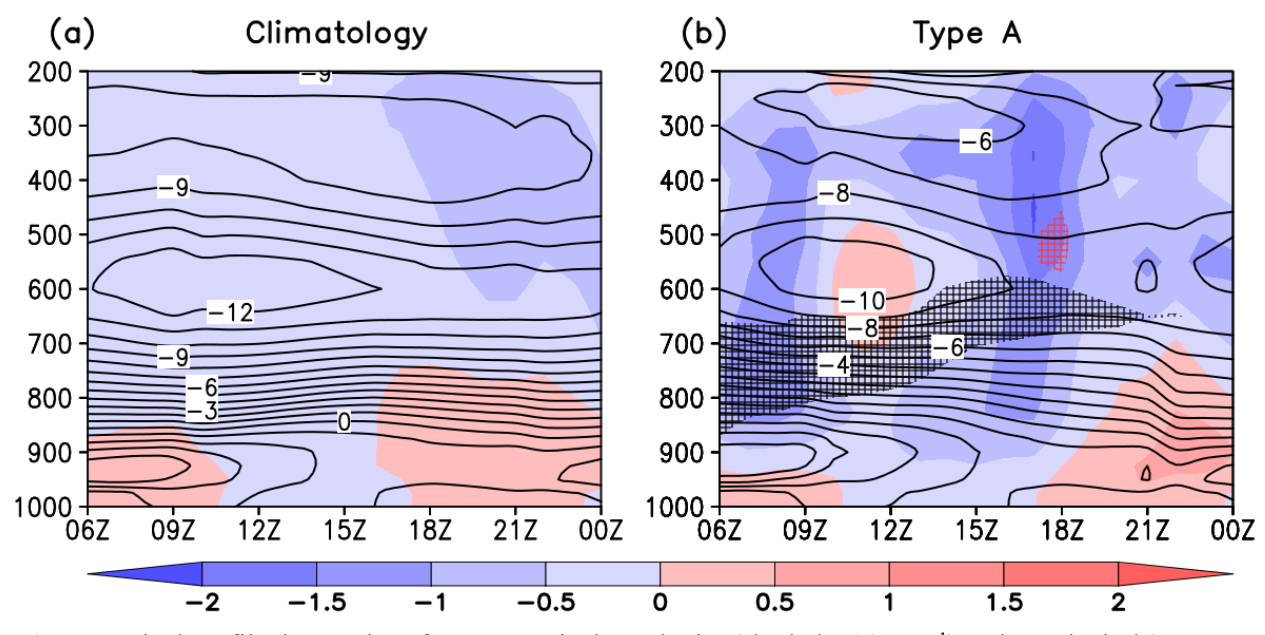


**Fig. 5** Vertical profile time series of ERA5 vertical-p velocity (shaded; x10 Pa s<sup>-1</sup>) and zonal wind (contours; m s<sup>-1</sup>) for the **(a)** weighted climatology and **(b)** Type A composite area-averaged over the Mali analysis region. Black (red) hatching denotes when the zonal wind (vertical-p velocity) difference Type A minus the weighted climatology is significant at the 90% level of confidence.

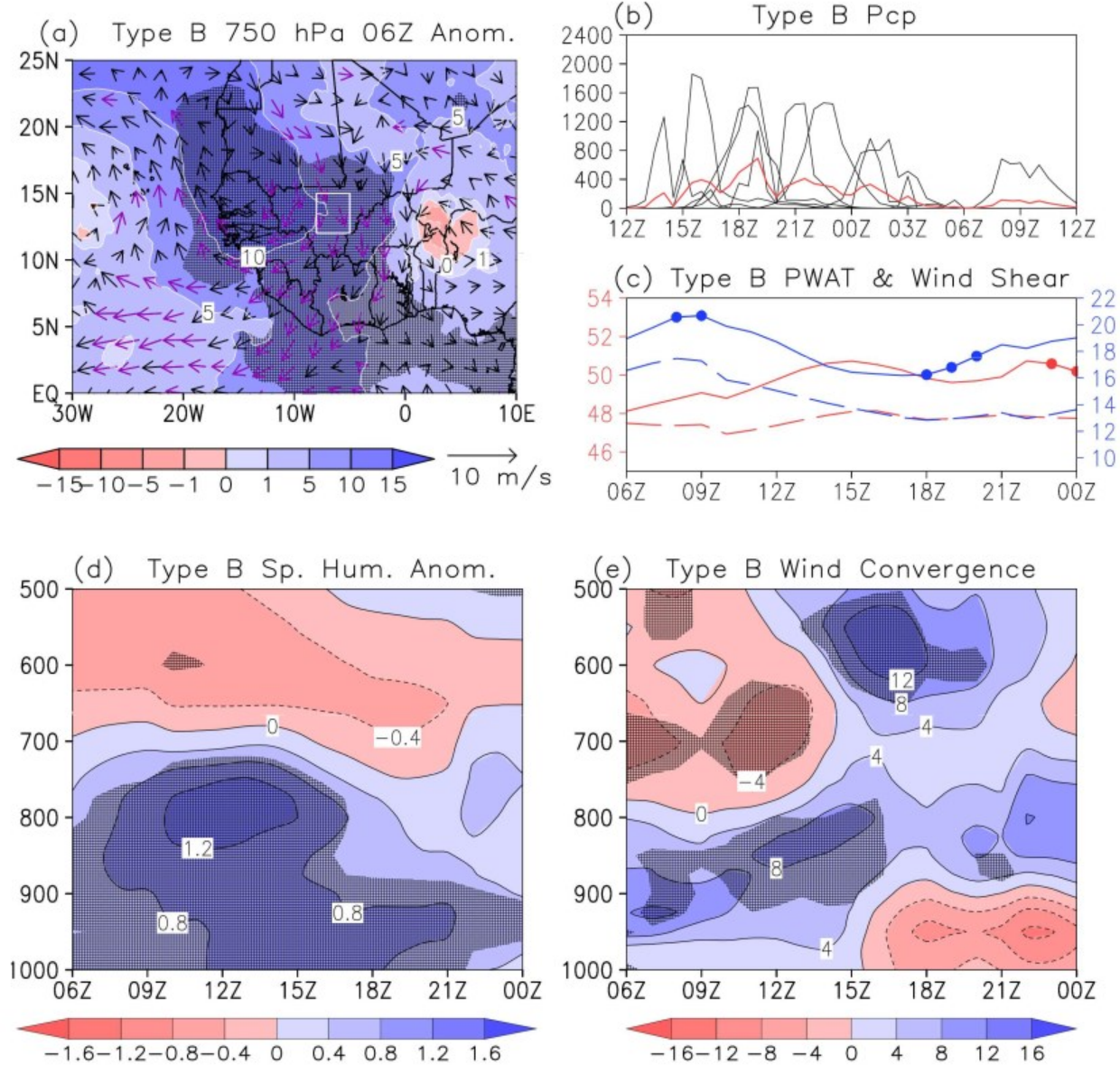


**Fig. 6** Type B **(a)** ERA5 06Z ( $t_0 - 6 h$ ) composite 750 hPa geopotential height (m) and wind (m s<sup>-1</sup>) anomalies. **(b)** IMERG rainfall rate (mm day<sup>-1</sup>) 12Z – 12Z time series for individual events at the maximum site locations (black lines) and the composite mean (red line). **(c)** ERA5 composite mean (solid lines) and the climatological (dashed lines) area-averaged precipitable water (red; mm) and 600 hPa – 925 hPa wind shear (m s<sup>-1</sup>; blue) time series over the Mali analysis region. Vertical profile time series of ERA5 area-averaged **(d)** specific humidity anomalies (g kg<sup>-1</sup>) and **(e)** absolute wind convergence (x10<sup>-6</sup> s<sup>-1</sup>) over the Mali analysis region. Hatching/dots/purple wind vectors denote significant differences from the weighted climatology at the 90% level of confidence.

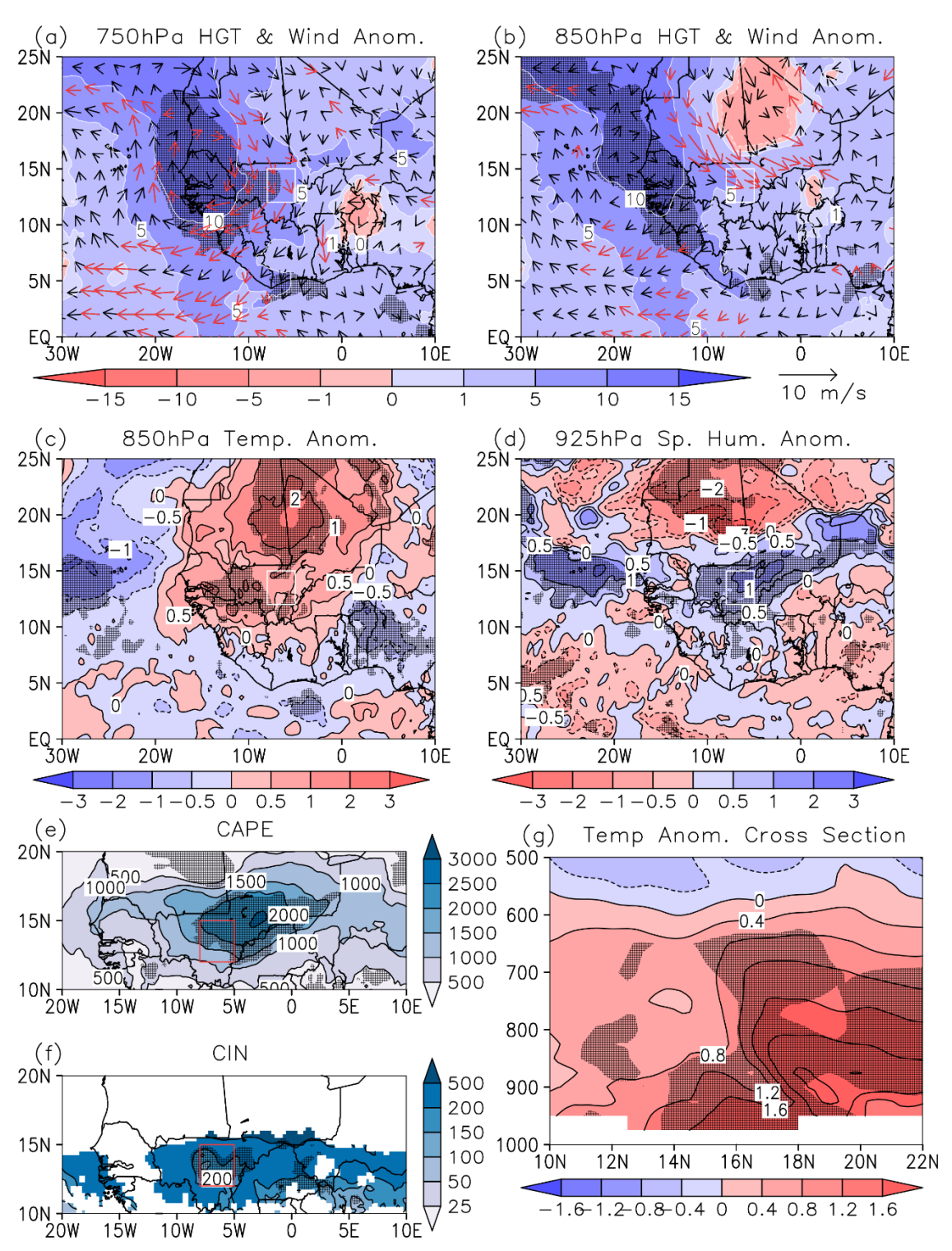


**Fig. 7** Type B ERA5 10Z ( $t_0 - 2h$ ) composite geopotential height (m) and wind (m s<sup>-1</sup>) anomalies at (a) 750 hPa and (b) 850 hPa, (c) 850 hPa temperature anomalies (K), (d) 925 hPa specific humidity anomalies (g kg<sup>-1</sup>), (e) CAPE (J kg<sup>-1</sup>) (f) CIN (J kg<sup>-1</sup>), and (g) vertical cross-section of temperature anomalies (K) averaged between 5°W - 8°W. Hatching/red vectors denote where the anomaly field is significant at the 90% level of confidence. Box denotes the location of the Mali analysis region.

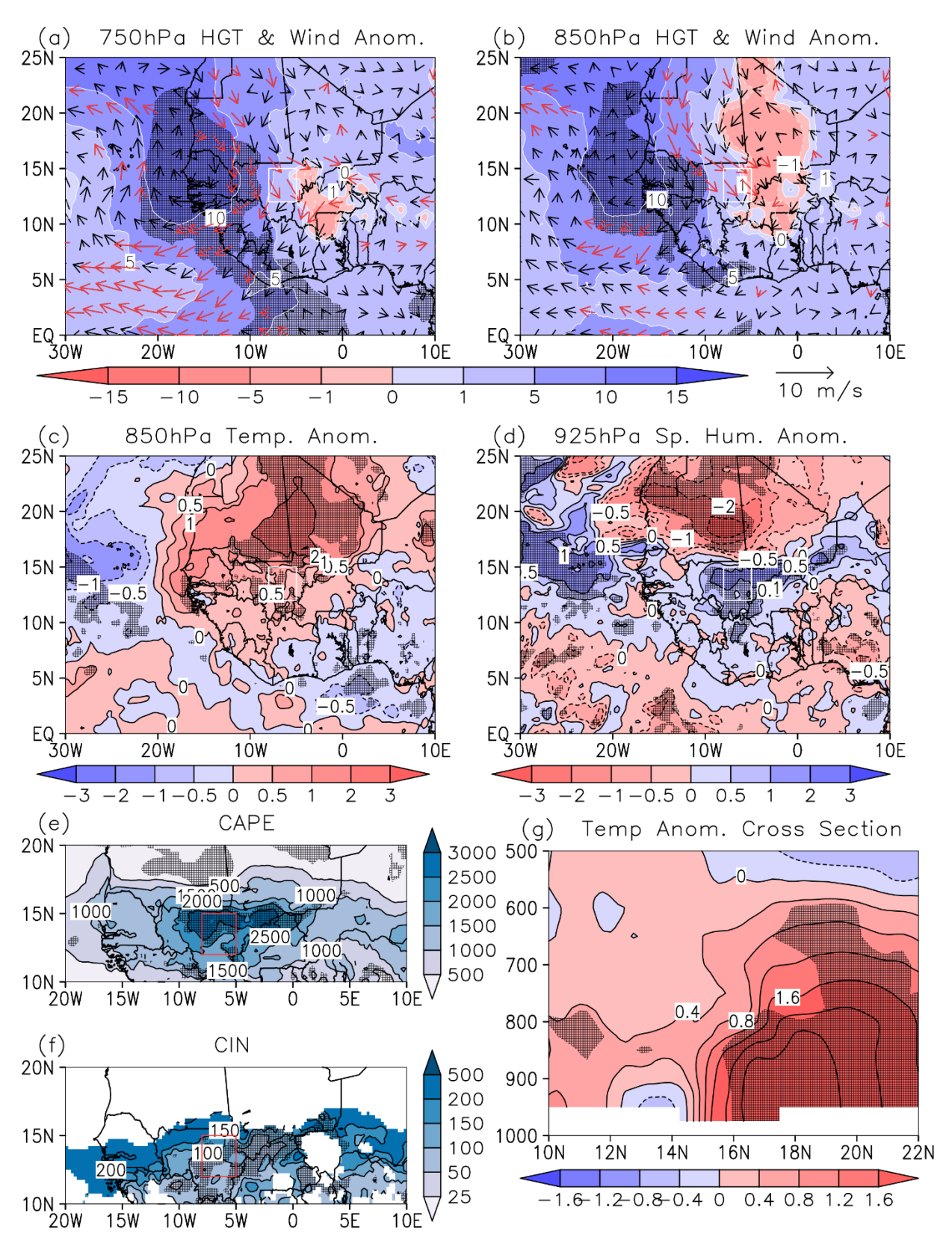


**Fig. 8** Same as Fig. 7 except at  $15Z(t_0 + 3h)$ .

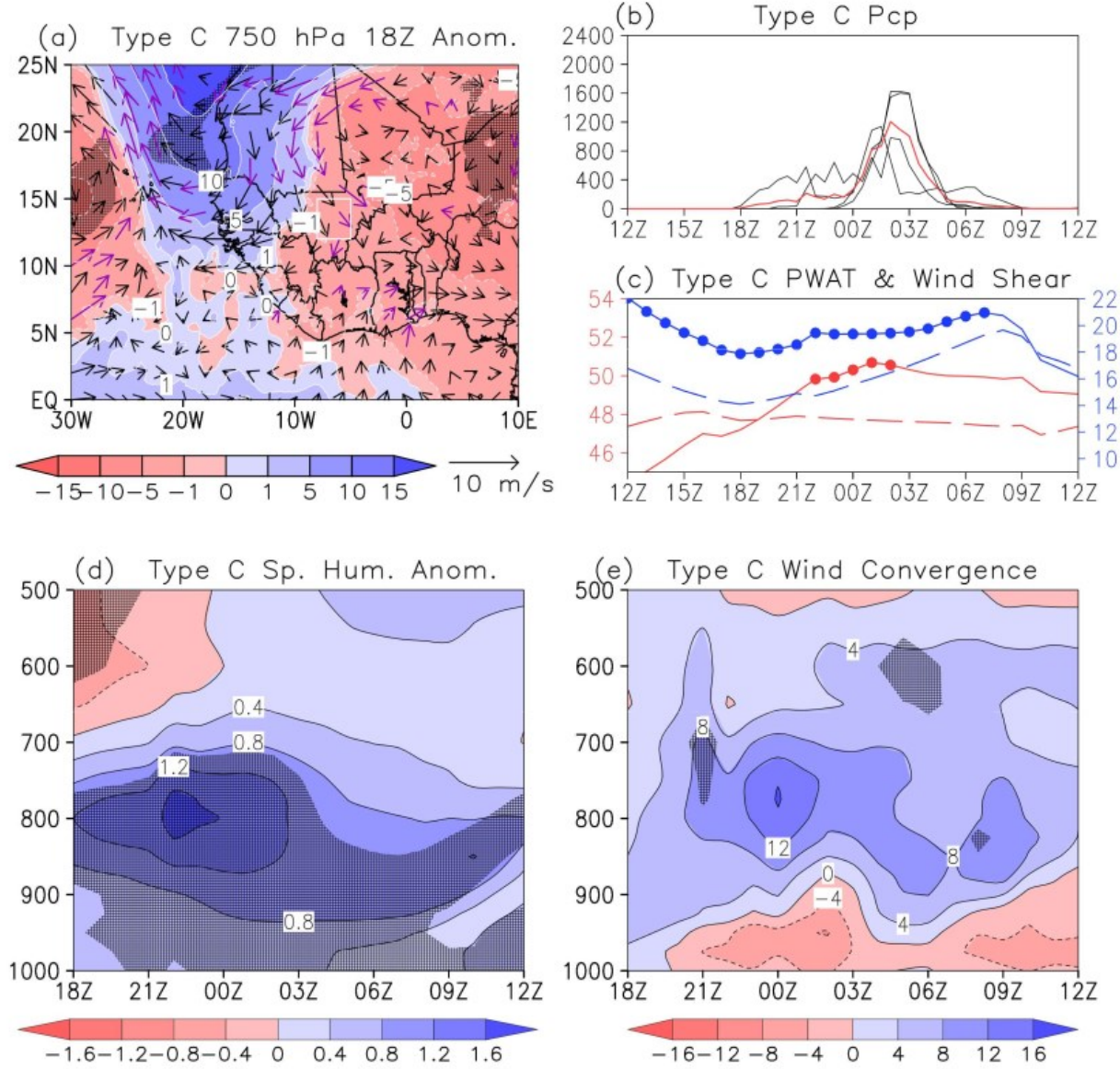


**Fig. 9** Type C (a) ERA5 18Z ( $t_0 + 6 h$ ) composite 750 hPa geopotential height (m) and wind (m s<sup>-1</sup>) anomalies. (b) IMERG rainfall rate (mm day<sup>-1</sup>) 12Z – 12Z time series for individual events at the maximum site locations (black lines) and the composite mean (red line). (c) ERA5 composite mean (solid lines) and the climatological (dashed lines) area-averaged precipitable water (red; mm) and 600 hPa – 925 hPa wind shear (m s<sup>-1</sup>; blue) time series over the Mali analysis region. Vertical profile time series of ERA5 area-averaged (d) specific humidity anomalies (g kg<sup>-1</sup>) and (e) absolute wind convergence (x10<sup>-6</sup> s<sup>-1</sup>) over the Mali analysis region. Hatching/dots/purple wind vectors denote significant differences from the weighted climatology at the 90% level of confidence.

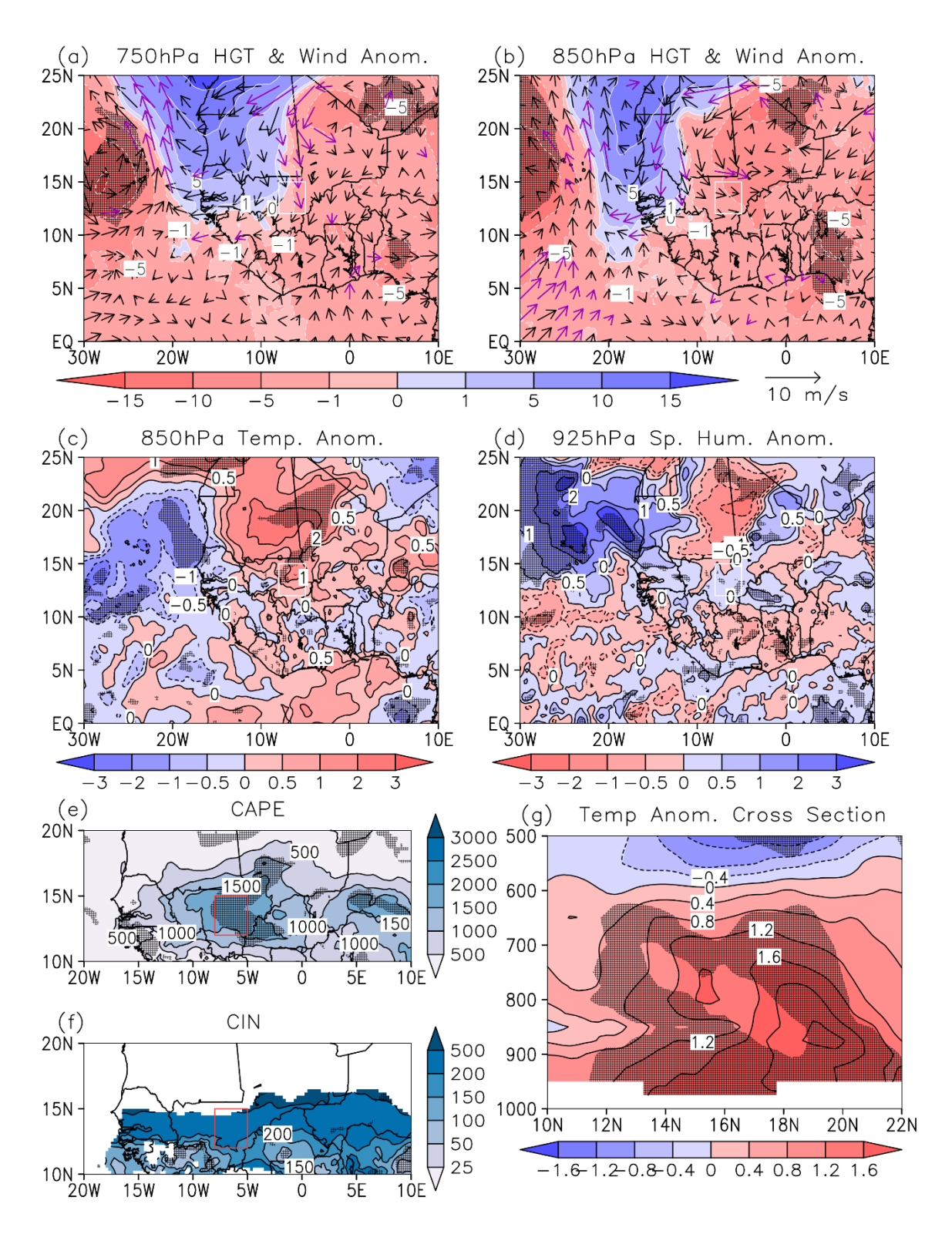


**Fig. 10** Type C ERA5 12Z ( $t_0$ ) composite geopotential height (m) and wind (m s<sup>-1</sup>) anomalies at **(a)** 750 hPa and **(b)** 850 hPa, **(c)** 850 hPa temperature anomalies (K), **(d)** 925 hPa specific humidity anomalies (g kg<sup>-1</sup>), **(e)** CAPE (J kg<sup>-1</sup>), **(f)** CIN (J kg<sup>-1</sup>) and **(g)** vertical cross-section of temperature anomalies (K) averaged between 5°W - 8°W. Hatching/purple vectors denote where the anomaly field is significant at the 90% level of confidence. Box denotes the location of the Mali analysis region.

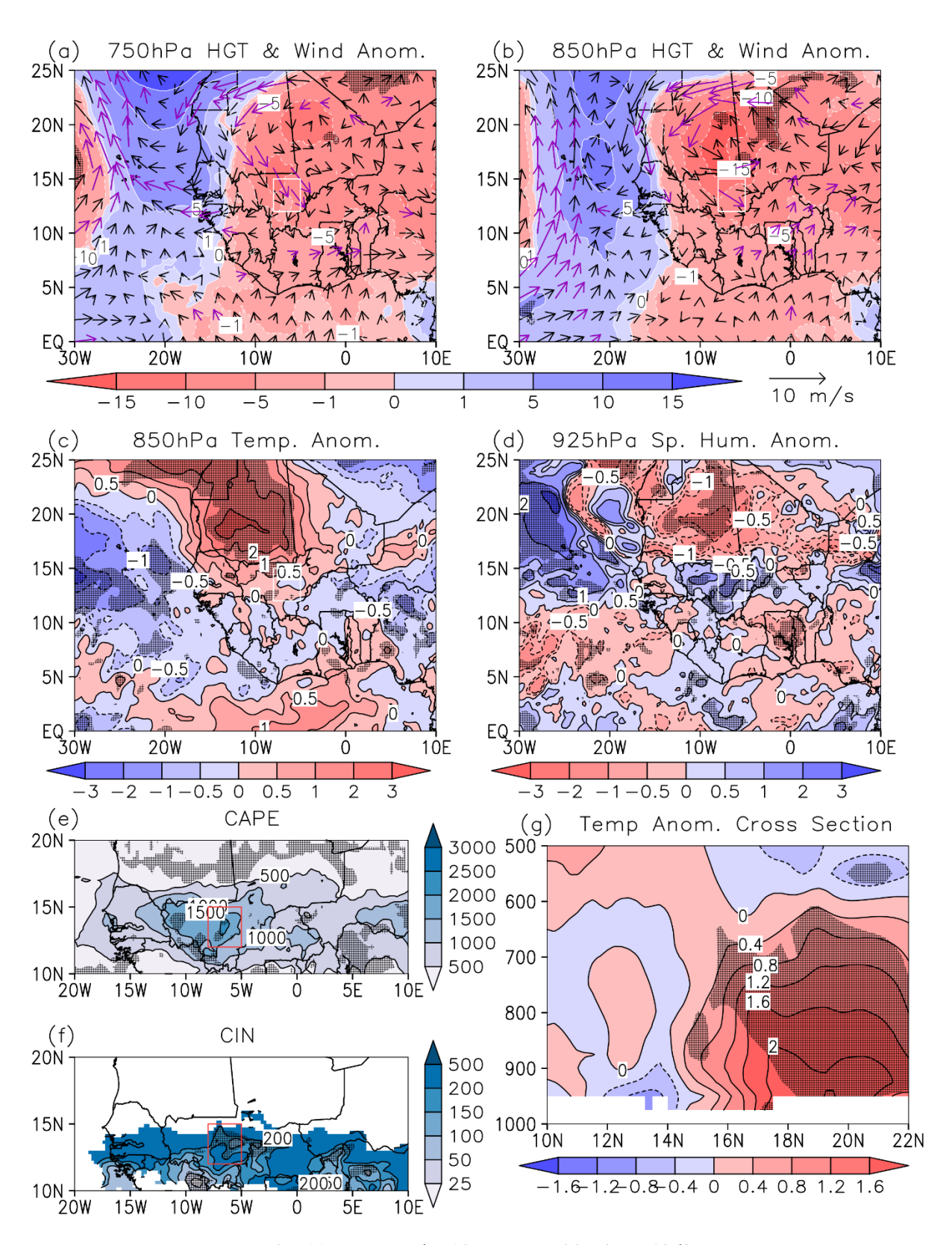


**Fig. 11** Same as Fig. 10 except at  $00Z (t_0 + 12 h)$ .

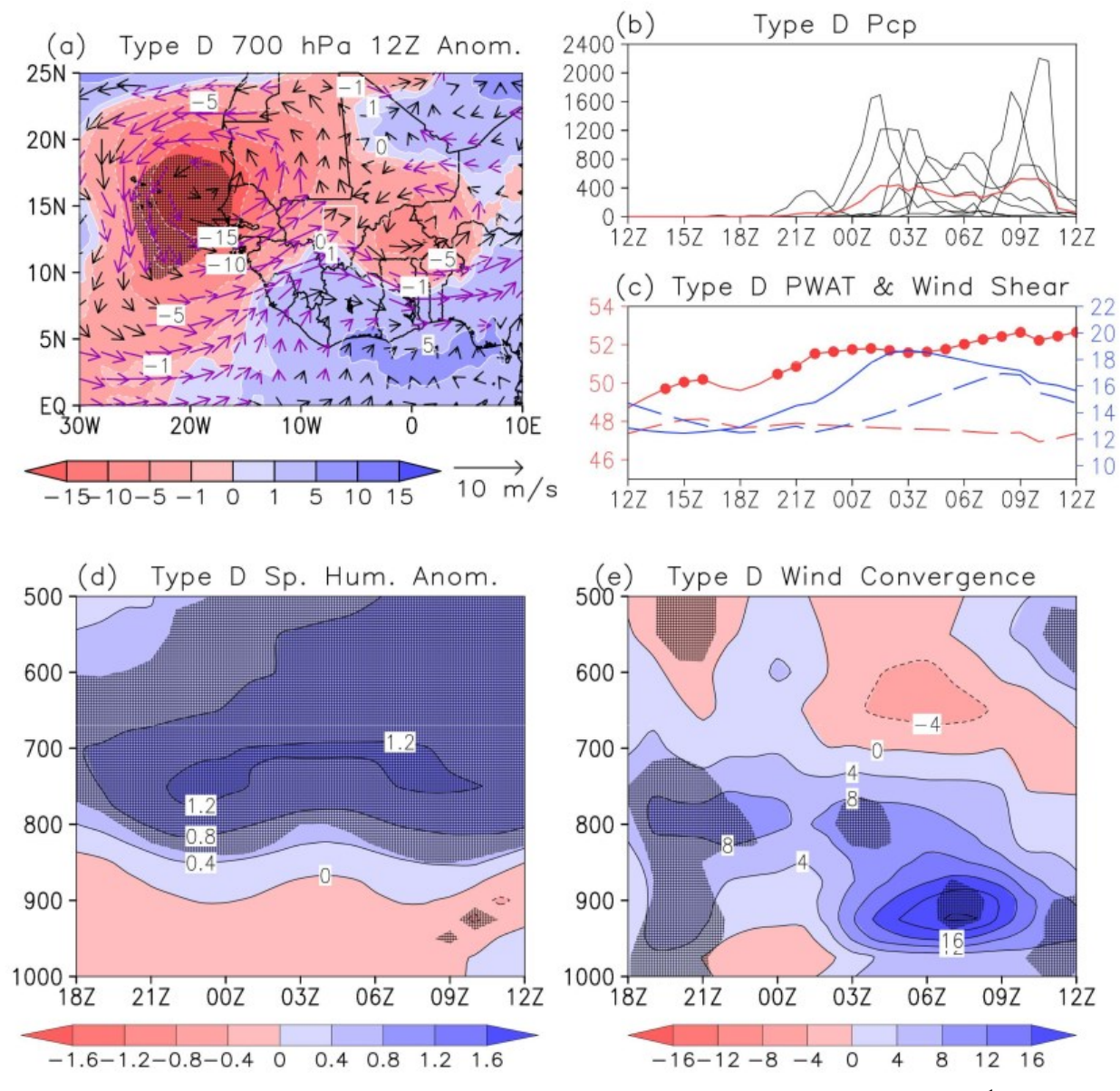


**Fig. 12** Type D (a) ERA5 12Z ( $t_0$ ) composite 700 hPa geopotential height (m) and wind (m s<sup>-1</sup>) anomalies. (b) IMERG rainfall rate (mm day<sup>-1</sup>) 12Z – 12Z time series for individual events at the maximum site locations (black lines) and the composite mean (red line). (c) ERA5 composite mean (solid lines) and the climatological (dashed lines) area-averaged precipitable water (red; mm) and 600 hPa – 925 hPa wind shear (m s<sup>-1</sup>; blue) time series over the Mali analysis region. Vertical profile time series of ERA5 area-averaged (d) specific humidity anomalies (g kg<sup>-1</sup>) and (e) absolute wind convergence (x10<sup>-6</sup> s<sup>-1</sup>) over the Mali analysis region. Hatching/dots/purple wind vectors denote significant differences from the weighted climatology at the 90% level of confidence.

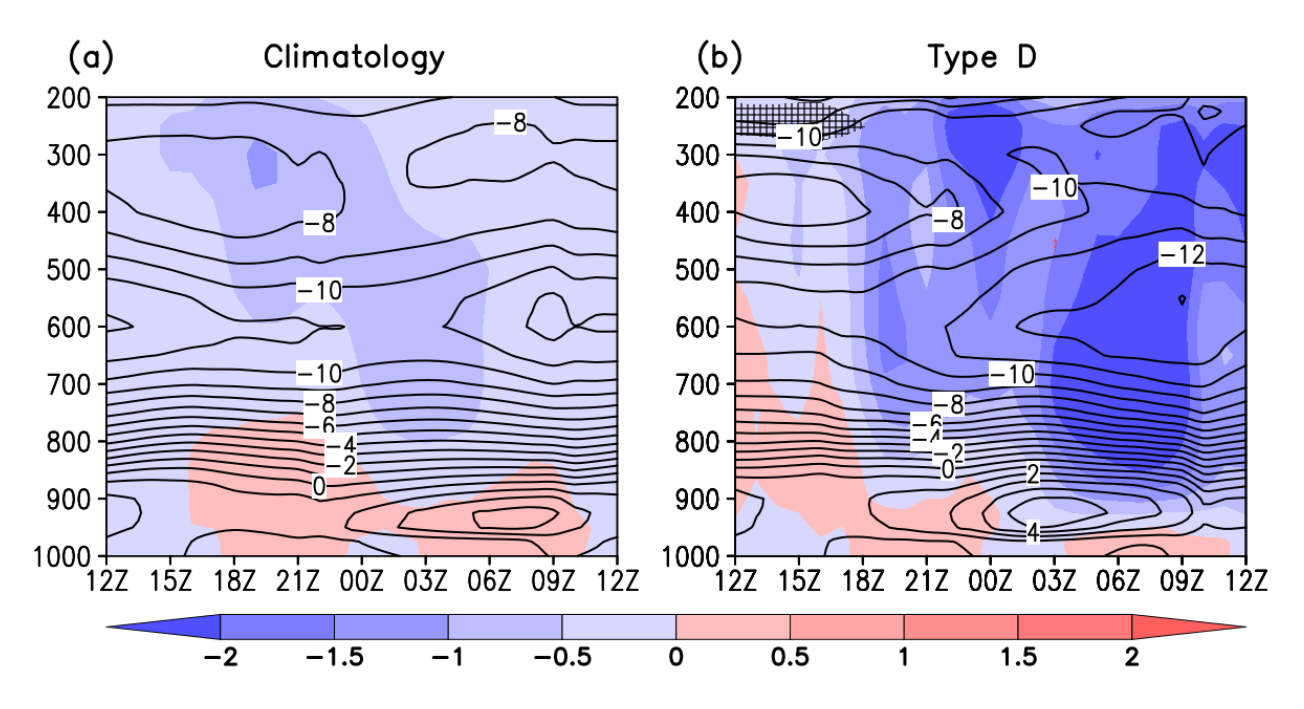


**Fig. 13** Vertical profile time series of ERA5 vertical-p velocity (shaded; x10 Pa s<sup>-1</sup>) and zonal wind (contours; m s<sup>-1</sup>) for the **(a)** weighted climatology and **(b)** Type D composite area-averaged over the Mali analysis region. Black (red) hatching denotes when the zonal wind (vertical-p velocity) difference Type D minus the weighted climatology is significant at the 90% level of confidence.

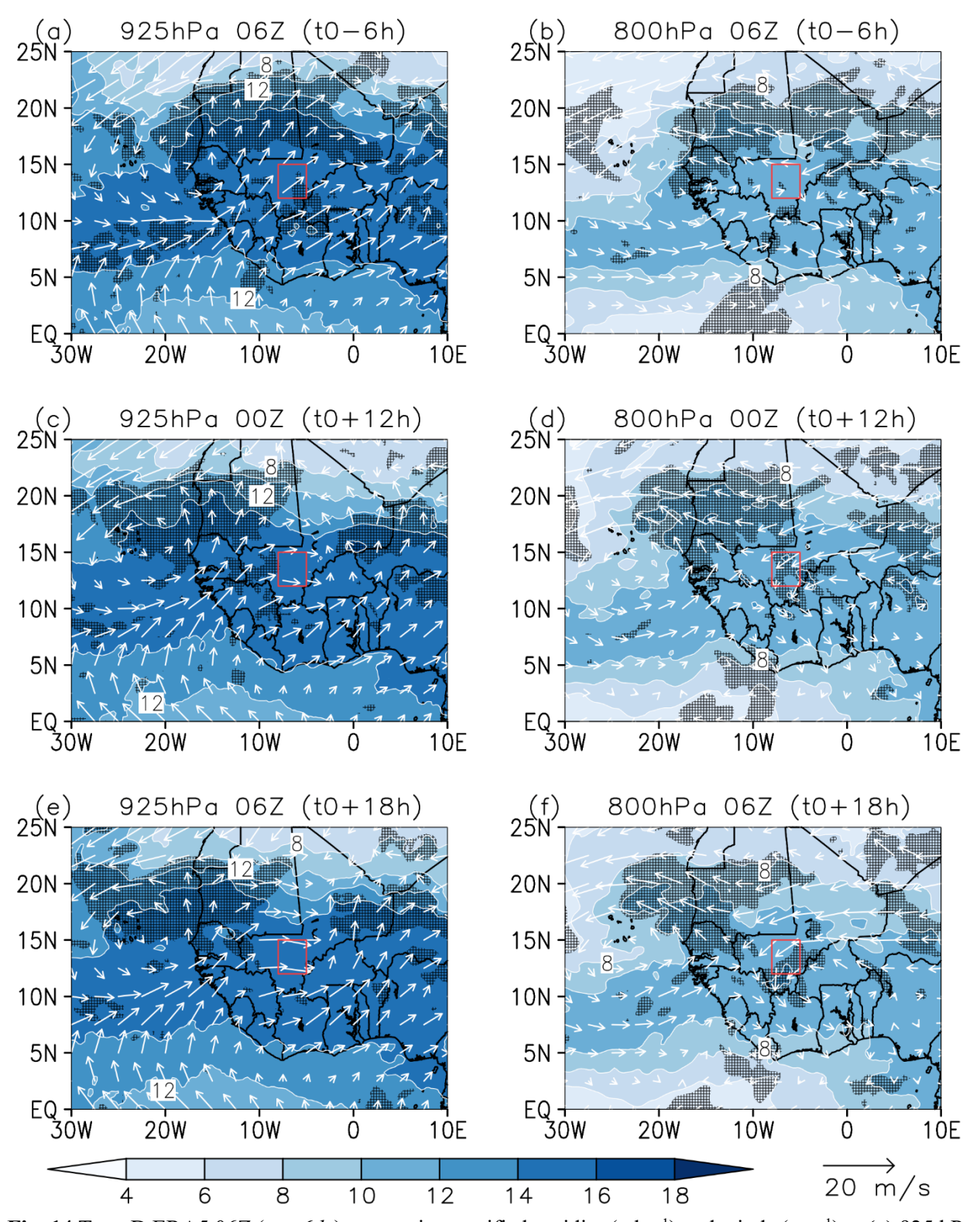


**Fig. 14** Type D ERA5  $06Z(t_0 - 6h)$  composite specific humidity (g kg<sup>-1</sup>) and winds (m s<sup>-1</sup>) at (a) 925 hPa and (b) 800 hPa, (c) & (d) and (e) & (f) are similar except they are for  $00Z(t_0 + 12h)$  and  $06Z(t_0 + 18h)$ , respectively. Hatching denotes areas that the specific humidity anomalies are significant at the 90% confidence level. Red box denotes Mali analysis region.

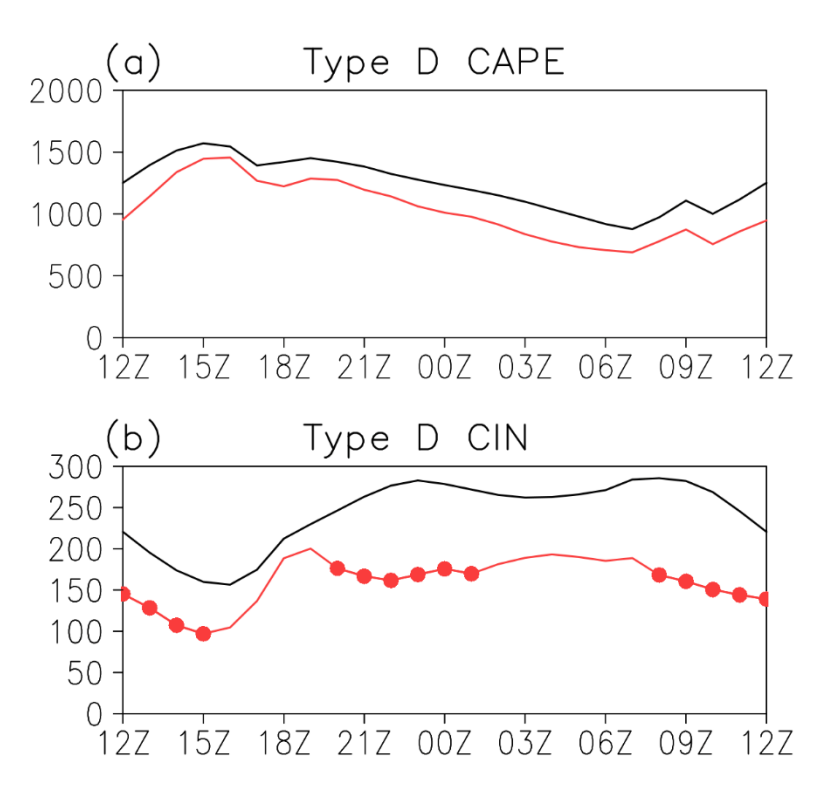


**Fig. 15** Time series of area-averaged **(a)** CAPE and **(b)** CIN over the Mali analysis region for the (black line) weighted climatology and (red line) Type D composite mean. Red dots denote significant differences from the weighted climatology at the 90% level of confidence.